Diabetes-induced Cellular Senescence and Senescence-Associated Secretory Phenotype Impair Cardiac Regeneration and Function Independently of Age

Fabiola Marino[1,2,#], Mariangela Scalise[1#], Nadia Salerno[3], Luca Salerno[1], Claudia Molinaro[3], Donato Cappetta[4], Michele Torella[5], Marta Greco[1], Daniela Foti[1], Ferdinando C. Sasso[5], Pasquale Mastroroberto[1], Antonella De Angelis[4], Georgina M. Ellison-Hughes[6], Maurilio Sampaolesi[2], Marcello Rota[7], Francesco Rossi[4], Konrad Urbanek[1], Bernardo Nadal-Ginard[3], Daniele Torella[1*], Eleonora Cianflone[3,7*]

Affiliations: [1]Department of Experimental and Clinical Medicine, Magna Graecia University, Catanzaro, 88100, Italy; [2]Translational Cardiomyology Laboratory, Stem Cell Biology and Embryology, Department of Development and Regeneration, KU Leuven, 3000 Leuven, Belgium; [3]Department of Medical and Surgical Sciences, Magna Graecia University, Catanzaro, 88100, Italy; [4]Department of Experimental Medicine, Section of Pharmacology, University of Campania "L.Vanvitelli", Naples, 80121, Italy; [5]Department of Translational Medicine, University of Campania "L.Vanvitelli", Naples, 80121, Italy; [6]Centre for Human and Applied Physiological Sciences and Centre for Stem Cells and Regenerative Medicine, School of Basic and Medical Biosciences, Faculty of Life Sciences & Medicine, King's College London, Guys Campus - SE1 1UL London, UK; [7]Department of Physiology, New York Medical College, Valhalla, NY, USA.

[#]*These two authors equally contributed to the present study*

***Correspondence to:** Daniele Torella, MD, PhD, e-mail: dtorella@unicz.it and/or Eleonora Cianflone, PhD, e-mail: cianflone@unicz.it

ABSTRACT

Diabetes Mellitus (DM) affects the biology of multipotent cardiac stem/progenitor cells (CSCs) and adult myocardial regeneration. We assessed the hypothesis that senescence and senescence-associated secretory phenotype (SASP) are a main mechanism of cardiac degenerative defect in DM. Accordingly, we tested whether that ablation of senescent CSCs would rescue the cardiac regenerative/reparative defect imposed by DM. We obtained cardiac tissue from non-aged (50-64 years old) DM type 2 (T2DM) and non-diabetic (NDM) patients with post-infarct cardiomyopathy undergoing cardiac surgery. A higher ROS production in T2DM associated with an increased number of senescent/dysfunctional T2DM-human(h)CSCs with reduced proliferation, clonogenesis/spherogenesis and myogenic differentiation vs. NDM-hCSCs *in vitro*. T2DM-hCSCs show a defined pathologic SASP. A combination of two senolytics, Dasatinib (D) and Quercetin (Q), clears senescent T2DM-hCSCs *in vitro* restoring their expansion and myogenic differentiation capacities. In a T2DM model in young mice, diabetic status *per se* (independently of ischemia and age) causes CSC senescence coupled with myocardial pathologic remodeling and cardiac dysfunction. D+Q treatment efficiently eliminates senescent cells, rescuing CSC function, which results in functional myocardial repair/regeneration improving cardiac function in murine DM. In conclusions, DM hampers CSC biology inhibiting their regenerative potential through the induction of cellular senescence and SASP independently from aging. Senolytics clear senescence abrogating the SASP restoring a fully proliferative-/differentiation- competent hCSC pool in T2DM with normalization of cardiac function.

Keywords: Senescence, Senescence-Associated Secretory Phenotype, Diabetes, Aging, Cardiac Stem/Progenitor Cells

INTRODUCTION

Aging is a major risk factor for the occurrence of several diseases, including stroke, myocardial infarction, heart failure, neurodegenerative disease, and several cancers. Therefore, the global rise in life expectancy will lead to a dramatic increase in age related diseases in the coming decades. In this scenario, cardiovascular diseases including atherosclerosis and heart failure (HF) increase exponentially with age, whereby HF is considered an epidemic because of a growing and ageing population. Type 2 diabetes mellitus (T2DM) is closely associated with aging and is a powerful independent risk factor for cardiovascular diseases such as atherosclerosis and heart failure [1]. This epidemiological connection between aging, T2DM, and cardiovascular diseases postulates the existence of a pathophysiological link.

Aging has been associated with systemic inflammation and oxidative stress [2], which can be both a cause as well as a consequence of DM [3]. Cellular senescence can be defined as a permanent arrest of cellular growth and is a key feature of aging [4,5]. Cell senescence is also a cause and a consequence of DM and plays an important role in its cardiovascular complications. Although senescent cells are classically reported as cells that irreversibly cease proliferation, they have the capacity to produce and secrete soluble factors that can influence neighboring cells and tissues [6,7]. This feature of senescent cells to secrete these soluble factors has taken the name of senescence-associated secretory phenotype (SASP) [8]. Since chronic inflammation is an important pathophysiological factor of both aging and diabetes, the SASP has been postulated as the pathophysiological link between aging and diabetes in cardiovascular diseases [9].

Tissue-specific adult stem cell senescence has emerged as an attractive theory for the decline in mammalian tissue and organ function during aging [10]. The mammalian heart, including the human, harbors a tissue specific cardiac stem/progenitor cell (CSC) compartment [11-15] that undergoes senescence with age, which dictates a progressive and permanent dysfunction of more than half of these endogenous cells by 75 years of age [5,10,16,17]. The senescent CSCs exhibit a SASP that can negatively impact surrounding cells, causing otherwise healthy and cycling-competent CSCs to lose

proliferative capacity and switch to a senescent phenotype. Nevertheless, even at the oldest age, it is still possible to retrieve a healthy, cycling-competent CSC fraction with an effective regenerative and reparative capacity [5,10,16]. Accordingly, experimental selective ablation of senescent CSCs either genetically or by a combination of senolytic drugs, fosters the expansion and functional regenerative recovery of the healthy aged CSCs [5,10,18].

Several reports have shown that DM impairs the *in vitro* proliferative and differentiation potential of CSCs [19-21]. Changes in chromatin conformation underlie the impaired proliferation, differentiation, and senescent behavior of diabetic CSCs [22]. Yet, it is unknown whether the SASP is induced by diabetes *per se* in CSCs and whether targeting senescent cells within the diabetic CSC compartment rescues their proliferation and differentiation defect in T2DM. Therefore, we assessed here the hypothesis that senescence and SASP are a main mechanism of cardiac degenerative defect in DM. Accordingly, we tested the hypothesis that ablation of senescent CSCs would rescue the cardiac regenerative/reparative defect imposed by DM. We show that the myocardium of T2DM patients, in a narrow age window of 55-64 years, undergoing cardiac surgery for ischemic heart disease, is characterized by an increased oxidative stress that affects the CSC compartment with an increased senescent phenotype when compared to myocardium and CSCs of age and sex matched NON-Diabetic Mellitus (NDM) patients. Importantly, T2DM CSCs have a SASP and senolytic treatment abrogate the senescent diabetic CSCs which allows healthy CSCs to proliferate and differentiate normally. Using a T2DM model in young mice, we further show that diabetic status *per se* (independently of ischemia and age) causes CSC senescence coupled with myocardial pathologic remodeling and cardiac dysfunction. Senolytic treatment efficiently eliminates senescent cells, rescuing CSC function, which results in functional myocardial repair/regeneration improving cardiac function in murine DM.

RESEARCH DESIGN AND METHODS

Patients Cohort and Samples

Human myocardial biopsies were obtained from Type 2 diabetes mellitus (T2DM) and NON-Diabetic Mellitus (NDM) patients with post-infarct cardiomyopathy which undergoing surgical coronary revascularization as previously described [23]. These biopsies were performed by the cardiac surgeons in an area immediately adjacent to macroscopically recognized infarcted tissue of the left ventricle. Collection of human tissues samples was approved by the local ethics committee at the University of Campania "L. Vanvitelli" of Naples and Magna Graecia University and performed in conformity with the principles outlined in the Declaration of Helsinki. Before cardiac surgery, written informed consent was obtained. All patient data were kept anonymous with no patient identifiers. As inclusion criteria an age between 50-64 years was required in order to try separate the effects of aging from Diabetes on senescence. We included 10 T2DM and 6 NDM patients from which peri-infarct/border zone biopsies were obtained (Supplementary Table 1). Freshly excised samples were formalin fixed for immunohistochemistry analysis as described below. Furthermore, additional 6 T2DM and 6 NDM patients with similar characteristics were included (Supplementary Table 1), from which atrial samples were obtained and processed for cell harvesting. Type 2 Diabetes Mellitus was defined in the presence of patients receiving stable glucose-lowering therapy and having a glycated hemoglobin level of at least 7.0%. Non-diabetic status was defined in the presence of normal glucose tolerance during a standard oral load glucose test, performed before coronary surgery.

Human CSCs Isolation and Culture

Human and mouse c-kit^{pos}CD45^{neg}CD31^{neg} CSCs (hCSCs) were obtained as previously described [12,15] and plated in CELL-Start (Life Technologies) or gelatin-coated dishes in complete CSC growth medium assembled as previously described [12,15]. For senolytic treatment, Dasatinib (D, LC Laboratories) and Quercetin (Q, Sigma-Aldrich) were used [5].

Animals

All animal experimental procedures were approved by Magna Greacia Institutional Review

Boards on Animal Use and Welfare. Mice were housed under controlled conditions of 25°C, 50% relative humidity and a 12 hr light (6:00 – 18:00) and 12 hr dark cycle, with water and food (containing 18.5% protein) available ad libitum, except for high fat diet (HFD, D12492) described below. Previously any invasive procedure, mice were anesthetized by intraperitoneal injections of Tiletamine/Zolazepam (80 mg/Kg) or inhaled isoflurane (isoflurane 1.5% oxygen 98.5%, Iso-Vet, Healthcare).

To induce T2DM in young mice, 6-weeks-old male and female C57/B6J mice (Charles River) were fed with a 60 kcal% high fat diet (HFD) for 2 weeks. During the third week mice received 4 consecutive daily injections of low dose Streptozotocin (STZ, 40 mg/kg intraperitoneal) dissolved in 0.05 M citrate buffer, pH 4 [24,25]. Control mice were fed with normal chow diet (NCD) or HFD without STZ. At 8 weeks of the experimental design, diabetic mice were randomized to Dasatinib (D, 5 mg/kg) + Quercetin (Q, 50 mg/kg) senolytic combination treatment (3 consecutive daily i.p. injection every week) or just placebo vehicle (Vehicle, i.p. injection) for four weeks. For the latter, D+Q were diluted in vehicle (50% PBS, 20%DMSO and 30% PEG-400). Additional vehicle-treated and D+Q treated diabetic mice were implanted subcutaneously (between the two scapulae) with mini-osmotic pumps (ALZET) to systemically release BrdU (50 mg/Kg/Day) for 28 days [15]. After 4 weeks were sacrificed and their hearts processed either for immunohistochemistry analysis or for CSC isolation. The complete animal study design *in vivo* with number of animals for each group is reported in Supplementary Figure 2.

Echocardiography

Echocardiography analysis were performed using Vevo 3100 system (Visualsonics, Inc.,) as previously reported. [26].

Histology and Immunohistochemistry

Human and mouse tissue specimens were fixed and embedded in paraffin or in Optimal Cutting Temperature Compound (OCT) for immunohistochemical analysis [5,12]. Sections were stained with

specific antibodies listed in Supplementary Table 2. Sections were examined by confocal microscopy (LEICA TCS SP8).

Immunohistochemical analysis of oxidative stress were performed using specific antibodies listed in Supplementary Table 2. The positive reactions were visualized using a Labelled Polymer-HRP complex and 3,3'-diaminobenzidine tetrahydrochloride (DAB) chromogen (EnVision+ Dual Link System-HRP, DAKO). Sections were then counterstained with hematoxylin and examined with light microscopy (LEICA, DMI3000B). For evaluation fibrosis, Picro Sirius Red staining was perfomed using manufacture's instructions (Bioptica).

FACS analysis

Cell analysis was performed on FACSCanto II (BD) with FlowJo software (TREE STAR) to identify the percentage of cardiac small cells expressing different cell-surface markers [12]. Specific antibodies used are listed in Supplementary Table 2. Ros generation was determinate using a CellRox Flow Cytometry Assay Kit (Life Technologies) according to the manufacture's instructions.

Proliferation, clonogenicity, cardiosphere formation and cardiomyocyte differentiation assays *in vitro*

Proliferation of hCSCs and mCSCs were evaluated through BrdU incorporation (10μM, Roche) and growth curve assays [5,12]. Single cell cloning was employed through depositing half-cell per well into 96-well CELL-Start-coated Terasaki plates [12]. For cardiosphere generation, $1x10^5$ hCSCs and mCSCs were placed in extra-low-attachment dishes in CSC growth medium [12].

For specific myogenic differentiation, hCSCs and mCSCs-derived-cardiospheres were placed in bacteriological dishes for 5-7 days for cardiospheres generation in CSC growth medium. Cardiospheres were then switched to base differentiation medium consisting of StemPro®-34 SFM (a serum-free medium conditioned with StemPro®-Nutrient Supplement, Gibco, Life Technologies), Glutamine (2mM) and penicillin-streptomycin (1%, Life Technologies) [12,27]. For specific myocyte differentiation BMP4 (10ng/ml, Peprotech), Activin-A (10 ng/ml first day and then 5ng/ml, Peprotech), β-FGF (10ng/ml, Peprotech), Wnt-11 (150ng/ml, R&D System) and Wnt-5a (150ng/ml,

R&D System) were added to base differentiation medium from day 0 to day 4. At day 4, differentiating cardiospheres were pelleted and transferred to laminin (1µg/ml) coated dishes and Dkk-1 (150ng/ml, R&D System) was added to base differentiation medium from day 5 to day 14 [12,27]. Differentiated mCSCs were trypsinized for RNA isolation.

From day 15 to day 28, the base differentiation medium for hCSCs were replaced by Gibco PSC Cardiomyocytes differentiation media (Thermo Fisher, A2921201) and differentiated CM-derived hCSCs were then either trypsinized for RNA isolation or fixed with 4% Paraformaldehyde (PFA, Sigma #P6148) and stained for cTnI and Actinin.

Immunocytochemistry

A volume of 200 µl of a 0.15×10^6 cells/ml suspension of CSCs were cytospun using a Shandon Cytospin 4 Cytocentrifuge (Thermo Fisher Scientific). Slides were immediately fixed using PFA 4% (Sigma-Aldrich). After fixation specific antibodies were used (Supplementary Table 2) [5].

Telomere length and Telomerase Activity Quantification

Genomic DNA of human T2DM-hCSCs and NDM-hCSCs was extracted using Quick-DNA Microprep Kit (Zymo Research). Telomere length was analyzed by using the Absolute Human Telomere Length Quantification qPCR Assay Kit (ScienCell Research Laboratories) [12]. T2DM-hCSCs and NDM-hCSCs were processed using the Telomerase Activity Quantification qPCR Assay Kit (ScienCell Research Laboratories) [12,28].

RNA extraction and RT-PCR analysis

RNA was extracted from T2DM-hCSCs and NDM-hCSCs, mouse CSCs isolated from vehicle or Q+D treated diabetic mice and CTRL mice using TRIzol® (Ambion). Reverse transcription was performed with 1-2 µg of RNA using HighCapacity cDNA Kit (Applied Biosystem). qRT-PCR was performed using TaqMan Primer/Probe sets (see Supplementary Table 3) using StepOne Plus real Time PCR System (Applied Biosystems).

Western Blot Analysis

Immunoblots were carried out using protein lysates obtained from T2DM-hCSCs and NDM-hCSCs as described [23], the relative antibodies listed in Supplementary Table 2.

Cytokine & growth factors assay

Cytokine and growth factor levels were simultaneously evaluated through the "Cytokine & Growth Factors Array (CTK)" kit (Randox Labs) by using Evidence Investigator biochip analyzer (Randox Labs) [29].

Statistical analysis

All data are presented in mean ± standard deviation. Data were analyzed using t-test comparisons in GraphPad Prism version 8.0.0 for Windows, GraphPad Software, San Diego, California USA, www.graphpad.com. Differences of $p<0,05$ are considered statistically significant.

Data and Resource Availability

All data generated or analyzed during this study are included in the published article (and its online supplementary files.

RESULTS

Increased Oxidative Stress in Diabetic Ischemic Cardiomyopathy

DM is characterized by an enhanced oxygen toxicity [30]. ROS is the distal signal of the cascade of events triggered by DM that leads to the initiation of the cell death pathway in the heart [31]. Human samples were thus analyzed for the presence of 8-OH-deoxyguanosine (8-OH-dG), Nitrotyrosine (3-NT), and 4-hydroxinonenal (4-HNE). T2DM resulted in an increase of myocardial cells positive for these markers of oxidative stress when compared to NDM patients (Figure 1A-C). In particular, a higher percentage of both cardiomyocytes and CSC-enriched c-kit^{pos}CD45^{neg}CD31^{neg} cardiac cells positive for 8-OH-dG and 3-NT, were detected in T2DM as compared with NDM (Figure 2A,B).

These data show that cardiac damage in T2DM is associated with a higher ROS production that targets both muscle cells as well as adult progenitor cells.

Increased Oxidative Stress Associated with Increased Expression of Senescent Markers in hCSCs from Diabetic Ischemic Cardiomyopathy

Cellular senescence is a cell state triggered by stressful insults and certain physiological processes, characterized by a prolonged and generally irreversible cell-cycle arrest with secretory features, macromolecular damage, and altered metabolism [32]. These alterations are generally inter-dependent as indeed oxygen toxicity and DNA damage alter telomeres, resulting in telomere shortening, cellular senescence, and cell dysfunction and/or death [32]. Although a link to organismal aging is clear, aging and senescence are not synonymous as, indeed, cells can undergo senescence, regardless of organismal age [33,34]. On the other hand, aging tissues experience a progressive decline in homeostatic and regenerative capacities, which has been attributed to senescence of their tissue-specific stem cells [35]. To assess whether the exaggerated ROS in T2DM is associated with senescence of tissue-resident CSCs, independently of age, we first assessed the expression of $p16^{INK4a}$ in CSCs-enriched c-$kit^{pos}CD45^{neg}CD31^{neg}$ cardiac cells in the myocardial sections from samples obtained from non-aged T2DM patients as compared to age-matched NDM patients. Indeed, $p16^{INK4a}$ is widely used as senescent biomarker, despite not being sufficient on its own to define/detect senescent cells [36-40].

The expression of $p16^{INK4a}$ in CSCs-enriched c-$kit^{pos}CD45^{neg}CD31^{neg}$ cardiac cells markedly increased in myocardial samples from T2DM ischemic cardiomyopathy when compared to NDM counterparts (Figure 2C), confirming that a higher myocardial oxidative stress couples with the induction of senescence in the cardiac progenitor pool.

To further assess senescence in the adult progenitor pool, we established cultures of human adult cardiac stem cells (hCSCs) from atrial specimens of T2DM (n=6) and NDM (n=6) patients undergoing cardiac surgery (Supplementary Table 1). c-$kit^{pos}CD45^{neg}CD31^{neg}$ cardiac cells from T2DM (hereafter T2DM-hCSCs) showed a membrane phenotype typical of cardiac cells enriched with multipotent hCSCs (Supplementary Figure 1A) as we have previously shown [12,41,42], with

no significant difference with c-kit^{pos}CD45^{neg}CD31^{neg} cardiac cells from NDM donors (hereafter NDM-hCSCs) (*data not shown*). Briefly, isolated T2DM-hCSCs, except for c-kit and CXCR4, are negative for the main human hematopoietic stem cell (hHSC) markers (namely CD45, CD34, CD38 and CD150). They are instead positive for several mesenchymal stem cell markers like CD90, CD105, CD166, CD73, CD13, CD29, CD44 and Stro-1 (Supplementary Figure 1A). A very small fraction of freshly isolated hCSCs also express pluripotency markers like OCT4 (2±2%), SOX2 (10±5%), NANOG (15±4%), KLF4 (8±3%) and cMYC (1±1%) and a small cell fraction expresses Sac2 (3±2%) (Supplementary Figure 1B).

In agreement with myocardial tissue assessment, T2DM-hCSCs at single cell level show increased ROS expression when compared to NDM-hCSCs (Figure 3A). As first assessment of replicative senescence in the isolated cells, we measured telomerase activity and telomeric length (Figure 3B). T2DM-hCSCs showed a significantly reduced telomerase activity, which associated with a decreased average telomere length when compared to NDM-hCSCs (Figure 3B). T2DM-hCSCs expressed biomarkers of cellular senescence at significantly higher levels than NDM-hCSCs. Indeed, T2DM-hCSCs had 10-times higher levels of p16^{INK4a} when compared to NDM-hCSCs (Figure 3C). Cytospin and immunocytochemistry at single cell level show that the number of p16^{INK4a}positive cells within c-kit^{pos}CD45^{neg}CD31^{neg} T2DM-hCSCs was significantly higher when compared to NDM-hCSCs (Figure 3D).

To strengthen the reliability of p16 expression in the identification of senescence, we assessed p21 and p53 expression in hCSCs from ND and T2-DM patients. The levels of p53, p21 and reactive oxygen species were all upregulated in T2DM-hCSCs when compared to ND-hCSCs (Figure 3C). Additionally, the majority of p16^{pos} T2DM-hCSCs were also positive for p21 (74±11%) (Figure 3E), lending support to the data that p16^{pos} cells represent true senescent cells. Concurrently, T2DM-hCSCs show increased senescence-associated beta-galactosidase (β-Gal) positive cells *in vitro* (Figure 3F). Furthermore, γ-H2AX expression revealed that T2DM-hCSCs accumulate significantly

more DNA damage than NDM-hCSCs *in vitro* (Figure 3G). Accordingly, T2DM-hCSCs had a significantly higher apoptotic rate when compared to NDM-hCSCs (Figure 3H).

These data suggest that T2DM produces exaggerated oxidative stress in hCSCs that is associated with replicative senescence markers, DNA damage, reduced telomerase activity and telomere shortening.

CSCs from non-aged diabetic subjects show impaired cell growth and myogenic differentiation potential *in vitro*

On the basis of the immunohistochemistry data showing increased $p16^{INK4a}$ expression in myocardial sections and of the *in vitro* data demonstrating telomerase deficit with telomere length attrition and increased p53, p21 and ROS levels, we evaluated freshly-isolated T2DM-hCSCs and NDM-hCSCs for their replicative competence and growth potential *in vitro*. T2DM-hCSCs show a significant decreased proliferation *in vitro* when compared to NDM-hCSCs, assessed either by growth curve kinetics over time or BrdU incorporation over 24 hours (Figure 4A,B). To determine whether the proliferation defect in the expansion capacity of T2DM-hCSCs was coupled with a deficit in other 'stemness' capabilities, we tested these cells for their clonal amplification at single cell level and for their spheroid formation potential in suspension [12]. At 14 days after cell deposition/plating in clonogenic or spherogenic medium, respectively, clonal efficiency and spherogenesis was 2.5-fold lower in T2DM-hCSCs compared to NDM-hCSCs (Figure 4C,D).

The above data show that T2DM increases senescence of hCSCs affecting their expansion, and clone/spheroid formation potential; we then tested the differentiation potential of these cells as it has been shown in different contexts that senescence and DM both affect differentiation of tissue-dependent stem/progenitor cells [19-21]. Considering that myogenic differentiation is key to myocardial repair/regeneration from endogenous progenitor cells, we specifically evaluated cardiomyocyte differentiation of T2DM-hCSCs vs. NDM-hCSCs grown in myogenic differentiation media [38]. RT-PCR data show that T2DM-hCSCs upregulated significantly less than NDM-hCSCs

the main cardiac transcription factors (GATA-4, NKX2.5 and MEF2C) and myocyte contractile genes (TNNT2, ACTC1, MYH6 and MYH7) during myogenic differentiation induction (Figure 4E). Only 24±4% and 25±6 of T2DM-hCSCs, as compared to 52±11% and 60±7% of NDM-hCSCs, respectively acquired the prototypical myocyte contractile markers cTnI and Actinin by 4 weeks in culture (Figure 4F,G). Furthermore, spontaneous beating of hCSC-derived cardiomyocytes *in vitro* as documentation of functional rhythmic contraction was consistently documented in NDM-hCSC-derived cardiomyocytes (Online Video 1) but seldomly detected in T2DM-hCSC-derived cardiomyocytes.

Overall, these data show that DM hampers human CSC biology, inducing a variety of hallmarks of senescence that contribute to the deficit of their regenerative potential.

T2DM-hCSCs exhibit a defined senescence-associated secretory phenotype (SASP)

Senescent cells secrete a plethora of factors, including pro-inflammatory cytokines and chemokines, growth modulators, angiogenic factors, and matrix metalloproteinases (MMPs), collectively known as the senescent associated secretory phenotype (SASP) [8,43]. The SASP constitutes a hallmark of senescent cells and mediates many of their patho-physiological effects, such as reinforcing and spreading senescence in autocrine and paracrine fashion [44], activating immune responses [45], hampering tissue plasticity [46] and contributing to persistent chronic inflammation (known as ”inflammaging”) [47]. Thus, the SASP explain several of the deleterious, pro-aging effects of senescent cells. On the other hand, all these patho-physiological mechanisms are equally active in DM. Therefore, we evaluated whether increased senescence markers and functional defect associated with SASP in T2DM-hCSCs.

To this aim, we obtained culture media from T2DM-hCSCs and NDM-hCSCs after 24 hours in serum-free conditions to evaluate production of several SASP factors, including MMP-3, PAI1, IL-6, IL-8, IL-1β and GM-CSF (Figure 5A,B). Interestingly, T2DM-hCSCs secreted respectively 10-, 7-, 18-, 54- and 56-fold higher amounts of IL-1A, IL-1β, IL-6, MCP-1 and IL-8, compared to NDM-

hCSCs (Figure 5A). Concurrently, mRNA levels of MCP1, IGFBP5, MMP3, IL-6, CCL-11, IL-8, GM-CSF and PAI1 SASP factors were all increased in T2DM-hCSCs vs. NDM-hCSCs (Figure 5B).

We then treated for 7 days NDM-hCSCs with conditioned medium (CoMe) derived from T2DM-hCSCs (T2DM-CoMe) and measured cell proliferation and senescence of the treated NDM-hCSCs. As controls, NDM-hCSCs were treated either with normal growth media or CoMe from parallel cultures of NDM-hCSCs. Treatment of NDM-hCSCs with T2DM-CoMe resulted in a decreased proliferation ($p < 0.05$) (Figure 5C,D) and an increased proportion of senescent $p16^{INK4a}$ positive ($p < 0.05$), β-Gal-positive and γ-H2AX-positive hCSCs compared to NDM-hCSCs in unconditioned medium (UnCoMe) or CoMe from NDM-hCSCs (Figure 5E).

Finally, we addressed whether hyperglycemia *per se* causes senescence, SASP, and functional impairment of hCSCs *in vitro*. For this aim, NDM-hCSCs were cultured for 10 days in high glucose (HG, 30 mM) or low/normal glucose (LG, 5.5 mM) conditions. HG significantly increased the number of $p16^{INK4a}$-positive (11±5%) and $β\text{-}Gal^{pos}$ (16±6%) NDM-hCSCs compared to LG (1±1 and 2%, respectively) (Figure 5F). The latter was associated with a significant increase of SASP factors (Figure 5G). Accordingly, HG significantly impaired expansion capacity of NDM-hCSCs (Figure 5H).

These data show for the first time that diabetic milieu, and hyperglycemia *per se*, induce SASP in hCSCs isolated from non-aged patients. SASP appears to negatively affect neighbor hCSCs whereby senescence begets senescence, suggesting that targeting senescent cells could improve CSC dysfunction in Diabetes.

Senolytics rescue the regenerative deficit of diabetic hCSCs

Because senescent cells contribute to the outcome of a variety of cardiac disease, including age-related and -unrelated cardiac diseases like anthracycline cardiotoxicity [5,48-40], much effort has been recently made to therapeutically target the detrimental effects of cellular senescence. Among the latter, senolytic drugs are agents that selectively induce apoptosis of only senescent cells by

overriding senescent cell anti-apoptotic pathways (SCAPs), specifically operative in senescent cells, while they are harmless to non-senescent healthy cells [5]. One of the most well studied senolytic therapeutic approaches is the combination of Dasatinib (D) and Quercetin (Q) [5]. D targets specific tyrosine kinases and other key SCAP elements. On the other hand, the flavonoid Q targets BCL-2 family members as well as HIF-1α and particular nodes in PI3-kinase and p21-related anti-apoptotic pathways [73]. Because D and Q target different SCAP nodes and do not target equally all senescent cell types, to extend the range of senescent cells targeted, the combination of D + Q has been used and proven effective in several mouse *in vivo* studies, including on senescence CSCs [5], and also in a first-in-man clinical trial [74].

Thus, T2DM-hCSCs were plated in 24-well dishes at 40% confluence and left for 2 days. Then, cells were administered with a combination of D+Q at a dose of 0.25 μM D with 10 μM Q. Six hours later, D+Q conditioned medium was replaced with complete fresh medium. Untreated cells served as controls. Two days later, D+Q treatment was repeated as above. Two days after, T2DM-hCSCs were analyzed for proliferation and markers of senescence, $p16^{INK4A}$, SA-β-gal and γ-H2AX. As shown in Figure 6, D+Q treatment removed from the cell culture the typical enlarged and flattened cell morphology of senescent cells, consistent with the senolytics combination targeting and removing senescent cells (Figure 6A). Concurrently, D+Q increased T2DM-hCSCs proliferation as evaluated by growth curve kinetics compared to untreated control T2DM-hCSCs (Figure 6B). Accordingly, D+Q significantly reduced the number of β-Gal and γ-H2AX positive T2DM-hCSCs as well as the number of $p16^{INK4a}$ senescent cells, which almost disappeared when compared to untreated T2DM-hCSCs (Figure 6C-E). Furthermore, we determined whether D+Q would abrogate the SASP in T2DM-hCSCs. We found that the level of SASP factors secreted by T2DM-hCSCs was significantly reduced by the administration of D+Q combination (Figure 6F).

Finally, considering that D+Q were able to ablate the senescent cells and the SASP from the T2DM-hCSC population, freeing the heatlhy non-senescent cells, we checked whether D+Q pre-treatment was able to rescue the altered myogenesis potential of T2DM-hCSCs. To that end, T2DM-

hCSCs were treated or untreated with D+Q as above in growth media and then cells were plated in bacteriological dishes for sphere formation [12]. CSC-derived cardiospheres were then plated in laminin for additional 7 days in the stage specific cardiomyogenic media [12]. Interestingly, D+Q pre-treatment restored the myogenic capacity of T2DM-hCSCs as indeed this senolytic combination significantly increased myogenic transcription factor and myogenic contractile gene expression as compared to untreated cells *in vitro* (Figure 6G). Accordingly, D+Q increased the number of T2DM-hCSC-derived cTnI^{pos} cardiomyocytes in differentiation media (Figure 6H).

Overall, these findings document that clearance of senescent cells using a combination of D+Q senolytics abrogates the SASP and restores a fully proliferative- and differentiation- competent hCSCs pool in T2DM.

Senolytics treatment *in vivo* removes senescent CSCs and improves cardiac repair and regeneration in diabetic mice

The above results using human samples and cells provide a strong proof of concept for senescence and SASP as main drivers of the cardiac regeneration deficit in DM, whose relevance was then translated and tested in a preclinical T2DM mouse model. 6-weeks-old C57/B6 mice started a 60 kcal% high fat diet (HFD) for 2 weeks and then on the third week they received 4 consecutive daily injections of low dose Streptozotocin (STZ, 40 mg/kg intraperitoneal) (Supplementary Figure 2A). These mice remained on the HFD until the completion of the study (Supplementary Figure 2A). Control (CTRL) mice were fed with normal chow diet (NCD) or HFD without STZ. Four weeks later, all animals treated with low dose STZ and on a HFD were diabetic showing altered fasting glycemia levels when compared to control mice (Supplementary Figure 2B). At this time point of the experimental design (8 weeks) eighteen mice were randomly assigned to be evaluated by echocardiography and six were sacrificed for cardiac histology and immunohistochemistry analysis (Supplementary Figure 2A). T2DM mice had normal ejection fraction but developed diastolic dysfunction with a significant reduction in early mitral annulus tissue velocity (E'wave, index of LV

myocardial relaxation in early diastole) and an increase in the ratio of early transmitral valve flow velocity (E wave) to E' wave (E/E′ ratio, an index of LV filling pressure) when compared to control (NCD and HFD) mice (Figure 7A,B), a classical feature of heart failure with preserved ejection fraction (HF-PEF) [51]. T2DM mouse hearts had an increased production of reactive oxygen species (Figure 7C) and an increased number of myocardial (interstitial) cell nuclei positive for p16 ^{INK4a} (2.25±0.93%) when compared to CTRL mice (0.07±0.02% and 0.07±0.07%, respectively for NCD and HFD) (Figure 7D). Furthermore, when compared to CTRL mouse hearts, T2DM hearts show increased cardiomyocyte (CM) apoptosis (1.33±0.4% vs. 0.01±0.01 and 0.01±0.01% for NCD and HFD, respectively) (Figure 7E) associated with reactive myocardial interstitial fibrosis (Figure 7F) and cardiomyocyte (CM) hypertrophy (Figure 7G). Intriguingly, at 8 weeks of the experimental design, T2DM hearts had 6.83±1.5% of their CSCs (identified as $CD45^{neg}CD31^{neg}c\text{-}kit^{pos}$ cardiac ells) positive for p16 ^{INK4a} when compared to 0.01±0.01% and 0.02±0.01% p16 ^{INK4a} -positive CSCs, respectively in NCD and HFD CTRL mice (Figure 7H). These data show that diabetic status *per se* (independently of age and ischemia) cause myocardial cell senescence including CSC senescence coupled with myocardial pathologic remodeling and cardiac dysfunction.

To address whether selectively eliminating senescent cells would improve cardiac function and repair in T2DM, the remaining T2DM mice (n=30) with HF-PEF were randomized to D+Q senolytic combination treatment (3 consecutive daily i.p. injection every week, n=15) or just placebo vehicle (Vehicle, i.p. injection, n=15) for four weeks. 6 placebo-treated and 6 D+Q treated diabetic mice were implanted subcutaneously (between the two scapulae) with mini-osmotic pumps to systemically release BrdU (50 mg/Kg/Day both) for 28 days to track myocardial cell regeneration. 4 weeks later, mice were assessed by Echocardiography (Supplementary Figure 2A), and the day after were sacrificed and their hearts processed for CSC isolation. Because of back skin pumps implants, mice with BrdU pumps were not included in the echocardiography study (Supplementary Figure 2A), and they were directly sacrificed at 4 weeks of treatment and processed for immunohistochemistry analysis. Echocardiography after 4 weeks shows that vehicle treated T2DM mice (n=9) had persistent

diastolic dysfunction when compared to CTRL mice (Figure 8A,B). Remarkably, D+Q treatment normalized diastolic dysfunction in T2DM mice (Figure 8B). D+Q treatment efficiently removed p16 ^{INK4a} -pos (0.5±0.14%) myocardial cells when compared to vehicle treatment (4.7±1.3%) in T2DM mice (Supplementary Figure 3A). The latter was associated with decreased cardiomyocyte apoptosis and reversal of cardiomyocyte hypertrophy in D+Q treated vs. vehicle T2DM diabetic mice (Supplementary Figure 3B,C). CSCs obtained from D+Q-treated mice showed a reduction of ROS levels compared to CSCs from CTRL and vehicle mice (Supplementary Figure 3D). Furthermore, D+Q combo treatment removed CSC p16 ^{INK4a} -pos senescent CSCs (0.1±0.07%) when compared to vehicle (10.7±1.5%) (Supplementary Figure 3E). Intriguingly, CSCs isolated from vehicle-treated T2DM mice show a defined SASP when compared to CSCs isolated from CTRL mice (Figure 8C). D+Q administration to T2DM mice significantly reduced SASP factors in CSCs (Figure 8C). CSCs isolated from placebo-treated T2DM mice show a reduced proliferation, clonal amplification, and myogenic differentiation *in vitro* when compared to CSCs from CTRL mice, consistent with T2DM imposing a senescence phenotype on CSCs (Figure 8D and Supplementary Figure 3F-H). *In vivo* D+Q administration eliminated CSC senescence phenotype, as indeed CSCs isolated from D+Q-combination treated T2DM mice show proliferation, clonal amplification and myogenic differentiation potential undistinguishable from CSCs from CTRL mice (Figure 8D and Supplementary Figure 3F-H). Finally, removal of both interstitial cardiac senescent cells and senescent CSCs by D+Q treatment resulted in an increased number of newly-generated BrdU^{pos} cardiomyocytes (1.2±0.31%) when compared to vehicle-treated (0.007±0.007%) T2DM mice (Figure 8E).

Overall, these data provide further evidence that diabetes per se causes myocardial cell senescence independently from age, affecting CSC regenerative potential, cardiac tissue composition and function. Accordingly, senolytics treatment efficiently eliminate senescent cells, rescuing CSC function, which results in functional myocardial repair and regeneration.

DISCUSSION

The main findings emanating from this study are that: i) myocardial tissue of non-aged T2DM patients with ischemic cardiomyopathy is characterized by an exaggerated oxidative stress targeting both cardiomyocytes and cardiac stem/progenitor cells (CSCs); ii) Increased oxidative stress in the myocardium of non-aged T2DM patients associates with an increased number of senescent and dysfunctional T2DM-hCSCs as shown by increased $p16^{INK4a}$, p53 and p21 expression, reduced telomerase activity and telomere length, reduced proliferation, clonogenesis/spherogenesis and myogenic differentiation; iii) T2DM-hCSCs from non-aged subjects show a senescence-associated secretory phenotype (SASP), as demonstrated by the increased secretion of several SASP factors, including MMP-3, PAI1, IL-6, IL-8, IL-1β and GM-CSF; iv) a combination of two senolytics, Dasatinib and Quercetin, clear senescent T2DM-hCSCs restoring expansion and myogenic differentiation capacities of the remaining diabetic hCSC pool; v) Diabetic cardiomyopathy in young mice, independently of age and ischemia, causes myocardial cell senescence, affecting CSC regenerative potential, cardiac tissue composition and function; vi) D+Q treatment *in vivo* removes senescent CSCs and improves cardiac repair, regeneration and function in diabetic mice.

T2DM is a pre-conditioning and powerful driver of organismal aging [52]. The biological foundations of aging primarily involve cellular senescence and T2DM is plethoric in senescence-driving factors [52]. An intense debate exists on whether senescence precedes or follows the onset of perpetual inflammation and insulin resistance (IR) in T2DM [53]. Independently from "*who-precedes-who*," diabetic patients experience an obvious accelerated aging process that increases their susceptibility to morbidity and earlier mortality mainly from cardiovascular disease [54, 55].

Adult tissue-specific stem cells are multipotent cells that are considered a lifelong cellular reservoir to ensure the continuous generation, replacement, and restitution of multiple tissue lineages [55,26]. However, during aging, these cells also undergo some detrimental changes such as alterations in the microenvironment, a decline in the regenerative capacity, and loss of function. So, aging has been linked to tissue-specific adult stem cell exhaustion [35]. Converging evidence conclusively

demonstrated how toxic high glucose load may be for survival, differentiation plasticity, and regenerative competence for different stem cells lineages [51,57-61]. The self-sustaining vicious circle of hyperglycemia/mitochondrial dysfunction/oxidative stress appears as a master driver to adult stem cell senescence [62]. Accordingly, the diabetic pro-oxidative environment is a major contributing factor for premature adult stem cell senescence and functional deficit [51,62-66]. Therefore, aging and T2DM drive adult stem cell senescence and regenerative deficit and conversely adult stem cell senescence and regenerative deficit drive the progressive pathology in aging and diabetes.

Like other tissue specific adult stem/progenitor cells, the CSCs are not immortal [16]. They undergo cellular senescence characterized by increased ROS production and oxidative stress and loss of telomere/telomerase integrity in response to a variety of physiological and pathological demands with aging [16]. Nevertheless, the old myocardium preserves an endogenous functionally competent CSC cohort which appears to be resistant to the senescent phenotype occurring with aging [16]. The latter envisions the phenomenon of CSC ageing as a result of a stochastic process, whereby targeting the senescent cells would benefit the recovery of a healthy CSC cohort [16]. Concurrently, T2DM impairs the *in vitro* proliferative and differentiation potential of human CSCs, worsening their senescence phenotype when compared with CSCs from non-diabetic ischemic patients [22]. Additionally, miR-34a is significantly upregulated while SIRT1 is downregulated in adult CSCs harvested from T2DM patients, which is associated with a higher pro-apoptotic caspase-3/7 activity [64]. All the above studies were, however, conducted in hCSCs isolated from diabetic old patients (>65 years), which could not clearly distinguish the role of age from DM on hCSC function. On the other hand, in an animal model of insulin-dependent DM in young mice, the myocardial accumulation of ROS drives CSC senescence through the expression of p53 and $p16^{INK4a}$ proteins and telomere erosion [31]. $p66^{shc}$ knockout inhibits CSC senescence and death, preventing the senescent phenotype and the development of cardiac failure by T2DM [31]. Additionally, DM persistently decreases the ability of isolated CSCs from young male mice to proliferate, survive oxidative insults, and

differentiate, which can be explained at least in part by an uncoupling of biosynthetic glucose metabolism pathways [67]. Altogether, these data postulate the tantalizing hypothesis that the premature cellular senescence of resident CSCs underpins the development of diabetic heart disease [10].

In the present study we provide evidence of the existence premature senescence of hCSCs in T2DM, demonstrating its functional relevance in the regenerative biology of these cells. Indeed, the elimination of senescent cells by senolytic treatment, a combination of Dasatinib and Quercetin, rescued the expansion and myogenic capacity of T2DM-hCSCs. Therefore, this data suggests that eliminating senescent hCSCs by senolytic therapy *in vivo* could be a therapeutic strategy to prevent CSC dysfunction even at early stages of diabetic disease.

Our findings on human CSCs are clearly hampered by the difficulty and limitation of working with samples of human tissue, which makes these data mainly descriptive and hypothesis-generating while falling short of being able to establish direct cause-effect relationship(s). Furthermore, to separate the effects of old age and diabetes on senescence, we chose an age cutoff of <65 years to define non-aged subjects, which might be seen as an arbitrary threshold when considering that WHO uses 60 years age as a cut off for predicting the shift in distribution of a country's population towards older ages – known as population ageing. Yet, old age in human beings is inconsistently defined from the standpoints of biology, demography (conditions of mortality and morbidity), employment and retirement, and sociology. As an example, in high-income countries setting at 60 years of age the threshold for aging is unrealistic because more than 30% of the relative population is already over 60 years old. Furthermore, several cardiovascular risk scores (and the CHA_2DS_2-VASc Score for thromboembolism in atrial fibrillation) use 65 years old to define aged/old people. Therefore, despite being imperfect, we chose this age cut-off. As a further limitation of the study on human samples we couldn't fully extrapolate the role of ischemic damage to the observed effects of T2DM on hCSC senescence *in vivo*. Indeed, DM is known to determine more intense microvascular ischemia and arterial dysfunction, which may have affected the status and function of hCSCs. Concurrently, short

leukocyte telomere length has been associated with plaque instability [68] and changes in several hemodynamic parameters such as impaired pressure-diameter relation, increased pulse pressure and pulse wave velocity, indicative of increased arterial stiffness [69-71]. When considering that telomere length shortening can be both a cause and effect of vascular disease, it is then possible that hCSC senescence within the myocardial microenvironment might be influenced by telomere dysregulation in the arterial system affected by diabetes. Despite all of the above, it should be noted that isolated hCSCs, diabetic and non-diabetic, were obtained from right atrial tissue which was not ischemic. Moreover, according to the "oxygen stem cell paradigm", adult stem cells are kept in niches with a very low O_2 concentrations [15]. Relevant to our study, it has been already shown that hypoxia (0.5%) O_2 reduces hCSC senescence and promotes their quiescence while long-term exposure to low oxygen levels (1%) increase hCSC proliferation, shifting their secretome to a more anti-inflammatory profile [72]. Finally, the diabetic milieu is a multifactorial environment constituted by several elements (high glucose, AGEs, angiotensin, and oxidative stress among others) that induce the expression of chemokines and adhesion molecules activating an inflammatory phenomenon linked to cell senescence [3]. All these elements therefore could be also responsible for the senescent cells in the myocardium of diabetic subjects.

Considering all the above limitations, through a reverse translational approach, we tested in a preclinical mouse model of T2DM the proof of concept provided by the human study that senescence and SASP are mechanistically linked to the cardiac regeneration defect of the diabetic adult myocardium, independently of age and ischemia. The murine data conclusively show that the working-hypothesis generated by the *in vitro* data on hCSC regenerative biology is indeed correct. T2DM in young mice causes CSC senescence and SASP, ensuing in a detrimental cardiac remodeling characterized by cardiomyocyte death and reduced regeneration owing to heart failure with preserved ejection fraction characterized by diastolic dysfunction at short/mid-term. Efficient removal of senescent cardiac cells, including senescent CSCs, by systemic administration of D+Q senolytic

combination restores CSC regenerative potential and cardiomyocyte regeneration, normalizing cardiac function in T2DM mice.

CONCLUSIONS

DM hampers CSC biology, inducing cellular senescence and senescence associate secretory phenotype (SASP) independently of age that contribute to a significant deficit of their regenerative potential and in particular to their ability to differentiate in new cardiomyocytes. Clearance of senescent cells by senolytics abrogates the SASP and restores a fully proliferative- and differentiation- competent hCSC pool in T2DM. Therefore, senolytics may represent a potential therapeutic approach to prevent or treat the reduced regenerative potential of the diabetic heart.

Funding: This research was funded by Grants from the Ministry of University and Research PRIN2015 2015ZTT5KB_004; PRIN2017NKB2N4_005; PON-AIM – 1829805-2

Duality of Interest: "The authors declare no conflict of interest."

Author contributions: Conceptualization: D.T., K.U. and E.C.; Design of the work: A.DeA., G.M.E-H.,K.U., D.T., and E.C. Data Acquisition and Analysis: F.M., M.S., L.S., D.C., C.M., N.S. M.G.; Interpretation: D.F., M.T., F.C.S, P.M., A.DeA., K.U., D.T., and E.C. Provided critical feedback and helped shape the research, analysis and manuscript.: M.S., F.R., G.M.E-H., and M.R. Writing original draft preparation and editing K.U., B.N-G., D.T and E.C. All of the authors approved the final version of this manuscript. D.T. and E.C. are the guarantors of this work and, as such, had full access to all of the data in the study and take responsibility for the integrity of the data and the accuracy of the data analysis.

REFERENCES:

1. Dunlay SM, Givertz MM, Aguilar D, Allen LA, Chan M, Desai AS, Deswal A, Vaughan Dickson V, Kosiborod MN, Lekavich CL, McCoy RG, Mentz RJ, Piña IL. Type 2 Diabetes

Mellitus and Heart Failure: A Scientific Statement From the American Heart Association and the Heart Failure Society of America. American Heart Association Heart Failure and Transplantation Committee of the Council on Clinical Cardiology; Council on Cardiovascular and Stroke Nursing and the Heart Failure Society of America. This statement does not represent an update of the 2017 ACC/AHA/HFSA heart failure guideline update. Circulation. 2019 Aug 13;140(7):e294-e324.

2. Gude NA, Broughton KM, Firouzi F, Sussman MA. Cardiac ageing: extrinsic and intrinsic factors in cellular renewal and senescence. Nat Rev Cardiol. 2018 Sep;15(9):523-542.
3. Halim M, Halim A. The effects of inflammation, aging and oxidative stress on the pathogenesis of diabetes mellitus (type 2 diabetes). Diabetes Metab Syndr. 2019;13(2):1165-1172.
4. van Deursen JM. The role of senescent cells in ageing. Nature. 2014 May 22; 509(7501):439-46.
5. Lewis-McDougall FC, Ruchaya PJ, Domenjo-Vila E, Shin Teoh T, Prata L, Cottle BJ, Clark JE, Punjabi PP, Awad W, Torella D, Tchkonia T, Kirkland JL, Ellison-Hughes GM. Aged-senescent cells contribute to impaired heart regeneration. Aging Cell. 2019 Jun;18(3):e12931.
6. Tchkonia, T, Zhu Y, van Deursen J, Campisi J, Kirkland JL. Cellular senescence and the senescent secretory phenotype: Therapeutic opportunities. The Journal of Clinical Investigation. 2013. 123(3), 966–972.
7. Xu M, Palmer AK, Ding H, Weivoda MM, Pirtskhalava T, White TA, Sepe A, Johnson KO, Stout MB, Giorgadze N, Jensen MD, LeBrasseur NK, Tchkonia T, Kirkland JL. Targeting senescent cells enhances adipogenesis and metabolic function in old age. Elife. 2015 Dec 19;4:e12997.
8. Acosta JC, Banito A, Wuestefeld T, Georgilis A, Janich P, Morton JP, Athineos D, Kang TW, Lasitschka F, Andrulis M, Pascual G, Morris KJ, Khan S, Jin H, Dharmalingam G, Snijders AP, Carroll T, Capper D, Pritchard C, Inman GJ, Longerich T, Sansom OJ, Benitah SA, Zender

L, Gil J. A complex secretory program orchestrated by the inflammasome controls paracrine senescence. Nat Cell Biol. 2013 Aug;15(8):978-90.

9. Shakeri H, Lemmens K, Gevaert AB, De Meyer GRY, Segers VFM. Cellular senescence links aging and diabetes in cardiovascular disease. Am J Physiol Heart Circ Physiol. 2018 Sep 1;315(3):H448-H462.
10. Cianflone E, Torella M, Biamonte F, De Angelis A, Urbanek K, Costanzo FS, Rota M, Ellison-Hughes GM, Torella D. Targeting Cardiac Stem Cell Senescence to Treat Cardiac Aging and Disease. Cells. 2020 Jun 26;9(6):1558.
11. Cianflone E, Aquila I, Scalise M, Marotta P, Torella M, Nadal-Ginard B, Torella D. Molecular basis of functional myogenic specification of Bona Fide multipotent adult cardiac stem cells. Cell Cycle. 2018;17(8):927-946.
12. Scalise M, Torella M, Marino F, Ravo M, Giurato G, Vicinanza C, Cianflone E, Mancuso T, Aquila I, Salerno L, Nassa G, Agosti V, De Angelis A, Urbanek K, Berrino L, Veltri P, Paolino D, Mastroroberto P, De Feo M, Viglietto G, Weisz A, Nadal-Ginard B, Ellison-Hughes GM, Torella D. Atrial myxomas arise from multipotent cardiac stem cells. Eur Heart J. 2020 Dec 1;41(45):4332-4345.
13. Scalise M, Marino F, Cianflone E, Mancuso T, Marotta P, Aquila I, Torella M, Nadal-Ginard B, Torella D. Heterogeneity of Adult Cardiac Stem Cells. Adv Exp Med Biol. 2019;1169:141-178.
14. Di Siena S, Gimmelli R, Nori SL, Barbagallo F, Campolo F, Dolci S, Rossi P, Venneri MA, Giannetta E, Gianfrilli D, Feigenbaum L, Lenzi A, Naro F, Cianflone E, Mancuso T, Torella D, Isidori AM, Pellegrini M. Activated c-Kit receptor in the heart promotes cardiac repair and regeneration after injury. Cell Death Dis. 2016 Jul 28;7(7):e2317.
15. Vicinanza C, Aquila I, Cianflone E, Scalise M, Marino F, Mancuso T, Fumagalli F, Giovannone ED, Cristiano F, Iaccino E, Marotta P, Torella A, Latini R, Agosti V, Veltri P, Urbanek K,

Isidori AM, Saur D, Indolfi C, Nadal-Ginard B, Torella D. Kit^{cre} knock-in mice fail to fate-map cardiac stem cells. Nature. 2018 Mar 21;555(7697):E1-E5.

16. Cianflone E, Torella M, Chimenti C, De Angelis A, Beltrami AP, Urbanek K, Rota M, Torella D. Adult Cardiac Stem Cell Aging: A Reversible Stochastic Phenomenon? Oxid Med Cell Longev. 2019 Feb 7;2019:5813147.
17. Marino F, Scalise M, Cianflone E, Mancuso T, Aquila I, Agosti V, Torella M, Paolino D, Mollace V, Nadal-Ginard B, Torella D. Role of c-Kit in Myocardial Regeneration and Aging. Front Endocrinol (Lausanne). 2019 Jun 19;10:371.
18. Tchkonia, T, Kirkland JL. Aging, cell senescence, and chronic disease: Emerging therapeutic strategies. JAMA. 2018;320(13), 1319–1320.
19. Zhang X, Meng K, Pu Y, Wang C, Chen Y, Wang L. Hyperglycemia Altered the Fate of Cardiac Stem Cells to Adipogenesis through Inhibiting the β-Catenin/TCF-4 Pathway. Cell Physiol Biochem. 2018;49(6):2254-2263.
20. She T, Wang X, Gan Y, Kuang D, Yue J, Ni J, Zhao X, Wang G. Hyperglycemia suppresses cardiac stem cell homing to peri-infarcted myocardium via regulation of ERK1/2 and p38 MAPK activities. Int J Mol Med. 2012 Dec;30(6):1313-20.
21. Molgat AS, Tilokee EL, Rafatian G, Vulesevic B, Ruel M, Milne R, Suuronen EJ, Davis DR. Hyperglycemia inhibits cardiac stem cell-mediated cardiac repair and angiogenic capacity. Circulation. 2014 Sep 9;130(11 Suppl 1):S70-6.
22. Vecellio M, Spallotta F, Nanni S, Colussi C, Cencioni C, Derlet A, Bassetti B, Tilenni M, Carena MC, Farsetti A, Sbardella G, Castellano S, Mai A, Martelli F, Pompilio G, Capogrossi MC, Rossini A, Dimmeler S, Zeiher A, Gaetano C. The histone acetylase activator pentadecylidenemalonate 1b rescues proliferation and differentiation in the human cardiac mesenchymal cells of type 2 diabetic patients. Diabetes. 2014 Jun;63(6):2132-47.
23. Torella D, Ellison GM, Torella M, Vicinanza C, Aquila I, Iaconetti C, Scalise M, Marino F, Henning BJ, Lewis FC, Gareri C, Lascar N, Cuda G, Salvatore T, Nappi G, Indolfi C, Torella

R, Cozzolino D, Sasso FC. Carbonic anhydrase activation is associated with worsened pathological remodeling in human ischemic diabetic cardiomyopathy. J Am Heart Assoc. 2014;3:e000434.

24. Luo J, Quan J, Tsai J, Hobensack CK, Sullivan C, Hector R, Reaven GM. Nongenetic mouse models of non-insulin-dependent diabetes mellitus. Metabolism. 1998 Jun;47(6):663-8. doi: 10.1016/s0026-0495(98)90027-0.
25. Tate M, Prakoso D, Willis AM, Peng C, Deo M, Qin CX, Walsh JL, Nash DM, Cohen CD, Rofe AK, Sharma A, Kiriazis H, Donner DG, De Haan JB, Watson AMD, De Blasio MJ, Ritchie RH. Characterising an Alternative Murine Model of Diabetic Cardiomyopathy. Front Physiol. 2019 Nov 14;10:1395. doi: 10.3389/fphys.2019.01395. Erratum in: Front Physiol. 2021 Aug 19;12:734320.
26. Aquila I, Cianflone E, Scalise M, Marino F, Mancuso T, Filardo A, Smith AJ, Cappetta D, De Angelis A, Urbanek K, Isidori AM, Torella M, Agosti V, Viglietto G, Nadal-Ginard B, Ellison-Hughes GM, Torella D. c-kit Haploinsufficiency impairs adult cardiac stem cell growth, myogenicity and myocardial regeneration. Cell Death Dis. 2019 Jun 4;10(6):436
27. Scalise M, Marino F, Salerno L, Mancuso T, Cappetta D, Barone A, Parrotta EI, Torella A, Palumbo D, Veltri P, De Angelis A, Berrino L, Rossi F, Weisz A, Rota M, Urbanek K, Nadal-Ginard B, Torella D, Cianflone E. In vitro CSC-derived cardiomyocytes exhibit the typical microRNA-mRNA blueprint of endogenous cardiomyocytes. Commun Biol. 2021 Sep 30;4(1):1146. doi: 10.1038/s42003-021-02677-y.
28. Xin H. Telomeric repeat amplification protocol: measuring the activity of the telomerase. Methods Mol Biol. 2011;735:107-11.
29. Accattato F, Greco M, Pullano SA, Carè I, Fiorillo AS, Pujia A, Montalcini T et al. Effects of acute physical exercise on oxidative stress and inflammatory status in young, sedentary obese subjects. PLoS One. 2017; 12(6): e0178900.

30. Pham-Huy LA, He H, Pham-Huy C. Free radicals, antioxidants in disease and health. Int J Biomed Sci. 2008 Jun;4(2):89-96.

31. Rota M, LeCapitaine N, Hosoda T, Boni A, De Angelis A, Padin-Iruegas ME, Esposito G, Vitale S, Urbanek K, Casarsa C, Giorgio M, Lüscher TF, Pelicci PG, Anversa P, Leri A, Kajstura J. Diabetes promotes cardiac stem cell aging and heart failure, which are prevented by deletion of the p66shc gene. Circ Res. 2006 Jul 7;99(1):42-52.

32. Coluzzi E, Colamartino M, Cozzi R, Leone S, Meneghini C, O'Callaghan N, Sgura A. Oxidative stress induces persistent telomeric DNA damage responsible for nuclear morphology change in mammalian cells. PLoS One. 2014 Oct 29;9(10):e110963.

33. Rodier F, Muñoz DP, Teachenor R, Chu V, Le O, Bhaumik D, Coppé JP, Campeau E, Beauséjour CM, Kim SH, Davalos AR, Campisi J. DNA-SCARS: distinct nuclear structures that sustain damage-induced senescence growth arrest and inflammatory cytokine secretion. J Cell Sci. 2011 Jan 1;124(Pt 1):68-81

34. Gorgoulis V, Adams PD, Alimonti A, Bennett DC, Bischof O, Bishop C, Campisi J, Collado M, Evangelou K, Ferbeyre G, Gil J, Hara E, Krizhanovsky V, Jurk D, Maier AB, Narita M, Niedernhofer L, Passos JF, Robbins PD, Schmitt CA, Sedivy J, Vougas K, von Zglinicki T, Zhou D, Serrano M, Demaria M. Cellular Senescence: Defining a Path Forward. Cell. 2019 Oct 31;179(4):813-827.

35. Oh J, Lee YD, Wagers AJ. Stem cell aging: mechanisms, regulators and therapeutic opportunities. Nat Med. 2014 Aug;20(8):870-80.

36. McConnell BB, Gregory FJ, Stott FJ, Hara E, Peters G. Induced expression of p16(INK4a) inhibits both CDK4- and CDK2-associated kinase activity by reassortment of cyclin-CDK-inhibitor complexes. Mol Cell Biol. 1999 Mar;19(3):1981-9.

37. Jeyapalan JC, Sedivy JM. Cellular senescence and organismal aging. Mechanisms of Ageing and Development. 2008; 129(7), 467–474.

38. Kirkland JL, Hollenberg CH, Gillon WS. Age, anatomic site, and the replication and differentiation of adipocyte precursors. American Journal of Physiology. 1990;258(2 Pt 1), C206–C210

39. Sharpless NE, DePinho RA. How stem cells age and why this makes us grow old. Nature Reviews Molecular Cell Biology. 2007;8, 703.

40. Liu JY, Souroullas GP, Diekman BO, Krishnamurthy J, Hall BM, Sorrentino JA, Parker JS, Sessions GA, Gudkov AV, Sharpless NE. Cells exhibiting strong p16INK4a promoter activation in vivo display features of senescence. Proc Natl Acad Sci U S A. 2019 Feb 12;116(7):2603-2611.

41. Vicinanza C, Aquila I, Scalise M, Cristiano F, Marino F, Cianflone E, Mancuso T, Marotta P, Sacco W, Lewis FC, Couch L, Shone V, Gritti G, Torella A, Smith AJ, Terracciano CM, Britti D, Veltri P, Indolfi C, Nadal-Ginard B, Ellison-Hughes GM, Torella D. Adult cardiac stem cells are multipotent and robustly myogenic: c-kit expression is necessary but not sufficient for their identification. Cell Death Differ. 2017 Dec;24(12):2101-2116.

42. Smith AJ, Lewis FC, Aquila I, Waring CD, Nocera A, Agosti V, Nadal-Ginard B, Torella D, Ellison GM. Isolation and characterization of resident endogenous c-Kit+ cardiac stem cells from the adult mouse and rat heart. Nat Protoc. 2014 Jul;9(7):1662-81.

43. Kumari R, Jat P. Mechanisms of Cellular Senescence: Cell Cycle Arrest and Senescence Associated Secretory Phenotype. Front Cell Dev Biol. 2021 Mar 29;9:645593.

44. Hoare M, Narita M. Transmitting senescence to the cell neighbourhood. Nat Cell Biol. 2013 Aug;15(8):887-9.

45. Burton DGA, Stolzing A. Cellular senescence: Immunosurveillance and future immunotherapy. Ageing Res Rev. 2018 May;43:17-25.

46. Ritschka B, Storer M, Mas A, Heinzmann F, Ortells MC, Morton JP, Sansom OJ, Zender L, Keyes WM. The senescence-associated secretory phenotype induces cellular plasticity and tissue regeneration. Genes Dev. 2017 Jan 15;31(2):172-183.

47. Franceschi C, Garagnani P, Vitale G, Capri M, Salvioli S. Inflammaging and 'Garb-aging'. Trends Endocrinol Metab. 2017 Mar;28(3):199-212.

48. Carresi C, Musolino V, Gliozzi M, Maiuolo J, Mollace R, Nucera S, Maretta A, Sergi D, Muscoli S, Gratteri S, Palma E, Bosco F, Giancotta C, Muscoli C, Marino F, Aquila I, Torella D, Romeo F, Mollace V. Anti-oxidant effect of bergamot polyphenolic fraction counteracts doxorubicin-induced cardiomyopathy: Role of autophagy and c-kit^{pos}CD45^{neg}CD31^{neg} cardiac stem cell activation. J Mol Cell Cardiol. 2018 Jun;119:10-18.

49. Piegari E, De Angelis A, Cappetta D, Russo R, Esposito G, Costantino S, Graiani G, Frati C, Prezioso L, Berrino L, Urbanek K, Quaini F, Rossi F. Doxorubicin induces senescence and impairs function of human cardiac progenitor cells. Basic Res Cardiol. 2013 Mar;108(2):334.

50. Cappetta D, De Angelis A, Sapio L, Prezioso L, Illiano M, Quaini F, Rossi F, Berrino L, Naviglio S, Urbanek K. Oxidative Stress and Cellular Response to Doxorubicin: A Common Factor in the Complex Milieu of Anthracycline Cardiotoxicity. Oxid Med Cell Longev. 2017;2017:1521020.

51. McHugh K, DeVore AD, Wu J, Matsouaka RA, Fonarow GC, Heidenreich PA, Yancy CW, Green JB, Altman N, Hernandez AF. Heart Failure With Preserved Ejection Fraction and Diabetes: JACC State-of-the-Art Review. J Am Coll Cardiol. 2019;73(5):602-611.

52. Berlanga-Acosta JA, Guillén-Nieto GE, Rodríguez-Rodríguez N, Mendoza-Mari Y, Bringas-Vega ML, Berlanga-Saez JO, García Del Barco Herrera D, Martinez-Jimenez I, Hernandez-Gutierrez S, Valdés-Sosa PA. Cellular Senescence as the Pathogenic Hub of Diabetes-Related Wound Chronicity. Front Endocrinol (Lausanne). 2020 Sep 16;11:573032.

53. Prattichizzo F, de Nigris V, La Sala L, Procopio AD, Olivieri F, Ceriello A. "Inflammaging" as a druggable target: a senescence-associated secretory phenotype-centered view of Type 2 diabetes. Oxid Med Cell Longev. 2016; 2016:1810327.

54. Perkisas S, Vandewoude M. Where frailty meets diabetes. Diabetes Metab Res Rev. 2016 Jan;32 Suppl 1:261-7.

55. Alison K. Wright, Evangelos Kontopantelis, Richard Emsley, Iain Buchan, Naveed Sattar, Martin K. Rutter, Darren M. Ashcroft. Life Expectancy and Cause-Specific Mortality in Type 2 Diabetes: A Population-Based Cohort Study Quantifying Relationships in Ethnic Subgroups. Diabetes Care Mar. 2017; 40 (3) 338-345

56. Andrzejewska A, Lukomska B, Janowski M. Concise Review: Mesenchymal Stem Cells: From Roots to Boost. Stem Cells. 2019 Jul;37(7):855-864.

57. Yang G, Jia Y, Li C, Cheng Q, Yue W, Pei X. Hyperglycemic stress impairs the stemness capacity of kidney stem cells in rats. PLoS ONE. 2015; 10:e0139607.

58. Dienelt A, zur Nieden NI. Hyperglycemia impairs skeletogenesis from embryonic stem cells by affecting osteoblast and osteoclast differentiation. Stem Cells Dev. 2011; 20:465–74.

59. Xu W, Yu W, Gao H, Wang L, Liu X, Wang Y. Effects of high glucose and high lipid on proliferation and apoptosis of human umbilical cord mensenchymal stem cells. Chin J Tissue Eng Res. 2012; 16:5001– 5.

60. Krankel N, Adams V, Linke A, Gielen S, Erbs S, Lenk K, et al. Hyperglycemia reduces survival and impairs function of circulating blood derived progenitor cells. Arterioscler Thromb Vasc Biol. 2005; 25:698– 703.

61. Torella D, Iaconetti C, Tarallo R, Marino F, Giurato G, Veneziano C, Aquila I, Scalise M, Mancuso T, Cianflone E, Valeriano C, Marotta P, Tammè L, Vicinanza C, Sasso FC, Cozzolino D, Torella M, Weisz A, Indolfi C. miRNA Regulation of the Hyperproliferative Phenotype of Vascular Smooth Muscle Cells in Diabetes. Diabetes. 2018 Dec;67(12):2554-2568.

62. Vono R, Jover Garcia E, Spinetti G, Madeddu P. Oxidative Stress in Mesenchymal Stem Cell Senescence: Regulation by Coding and Noncoding RNAs. Antioxid Redox Signal. 2018 Sep 20;29(9):864-879.

63. Cassidy FC, Shortiss C, Murphy CG, Kearns SR, Curtin W, De Buitléir C, O'Brien T, Coleman CM. Impact of Type 2 Diabetes Mellitus on Human Bone Marrow Stromal Cell Number and Phenotypic Characteristics. Int J Mol Sci. 2020 Apr 2;21(7):2476.

64. Ko KI, Coimbra LS, Tian C, Alblowi J, Kayal RA, Einhorn TA, Gerstenfeld LC, Pignolo RJ, Graves DT. Diabetes reduces mesenchymal stem cells in fracture healing through a TNFalpha-mediated mechanism. Diabetologia. 2015; 58:633– 42.

65. van de Vyver M, Niesler C, Myburgh KH, Ferris WF. Delayed wound healing and dysregulation of IL6/STAT3 signalling in MSCs derived from pre-diabetic obese mice. Mol Cell Endocrinol. 2016; 426:1– 10.

66. Lu H, Wu X, Wang Z, Li L, Chen W, Yang M, Huo D, Zeng W, Zhu C. Erythropoietin-activated mesenchymal stem cells promote healing ulcers by improving microenvironment. J Surg Res. 2016; 205:464–73.

67. Fomison-Nurse I, Saw EEL, Gandhi S, Munasinghe PE, Van Hout I, Williams MJA, Galvin I, Bunton R, Davis P, Cameron V, Katare R. Diabetes induces the activation of pro-ageing miR-34a in the heart, but has differential effects on cardiomyocytes and cardiac progenitor cells. Cell Death Differ. 2018;25:1336–1349.

68. De Meyer T, Nawrot T, Bekaert S, De Buyzere ML, Rietzschel ER, Andrés V. Telomere Length as Cardiovascular Aging Biomarker: JACC Review Topic of the Week. J Am Coll Cardiol. 2018;72(7):805-813.

69. Peng H, Zhu Y, Yeh F, Cole SA, Best LG, Lin J, Blackburn E, Devereux RB, Roman MJ, Lee ET, Howard BV, Zhao J. Impact of biological aging on arterial aging in American Indians: findings from the Strong Heart Family Study. Aging (Albany NY). 2016 Aug;8(8):1583-92.

70. Benetos A, Okuda K, Lajemi M, Kimura M, Thomas F, Skurnick J, Labat C, Bean K, Aviv A. Telomere length as an indicator of biological aging: the gender effect and relation with pulse pressure and pulse wave velocity. Hypertension. 2001 Feb;37(2 Pt 2):381-5.

71. Honkonen M, Vääräniemi K, Saijonmaa O, Nyman A, Tikkakoski AJ, Koskela J, Lehtimäki T, Kähönen M, Mustonen J, Fyhrquist F, Pörsti I. Leukocyte telomere length is inversely associated with arterial wave reflection in 566 normotensive and never-treated hypertensive subjects. Aging (Albany NY). 2020 Jun 23;12(12):12376-12392.

72. Bellio MA, Rodrigues CO, Landin AM, Hatzistergos KE, Kuznetsov J, Florea V, Valasaki K, Khan A, Hare JM, Schulman IH. Physiological and hypoxic oxygen concentration differentially regulates human c-Kit+ cardiac stem cell proliferation and migration. Am J Physiol Heart Circ Physiol. 2016 Dec 1;311(6):H1509-H1519.

73. Wissler Gerdes EO, Zhu Y, Tchkonia T, Kirkland JL Discovery, development, and future application of senolytics: theories and predictions. FEBS J. 2020 Jun;287(12):2418-2427.

74. Hickson LJ, Langhi Prata LGP, Bobart SA, Evans TK, Giorgadze N, Hashmi SK, Herrmann SM, Jensen MD, Jia Q, Jordan KL, Kellogg TA, Khosla S, Koerber DM, Lagnado AB, Lawson DK, LeBrasseur NK, Lerman LO, McDonald KM, McKenzie TJ, Passos JF, Pignolo RJ, Pirtskhalava T, Saadiq IM, Schaefer KK, Textor SC, Victorelli SG, Volkman TL, Xue A, Wentworth MA, Wissler Gerdes EO, Zhu Y, Tchkonia T, Kirkland JL. Senolytics decrease senescent cells in humans: Preliminary report from a clinical trial of Dasatinib plus Quercetin in individuals with diabetic kidney disease. EBioMedicine. 2019 Sep;47:446-456.

FIGURE LEGENDS

Figure 1. Cardiac damage in diabetes is associated with higher ROS production. (A-C) Light microscopy images show representative DAB-staining of LV samples obtained from T2DM and NDM patients. The respective bar graph show (**A**) the percentage of 8-OH-dG positive nuclei (in brown), (**B**) the percentage of 3-NT positive cells (in brown) and (**C**) the 4-HNE intensity levels (in brown) in T2DM cross section compared to NDM tissue sections (n=10 T2DM heart sections and n=6 NDM heart sections). Scale bar= 200μm. All data are mean±S.D.

Figure 2. Quantification of oxidative stress and senescent markers in myocytes and progenitor cells. (**A**) Representative confocal images and bar graph showing 8-OH-dG positive cardiomyocytes and 8-OH-dG positive hCSCs in LV samples obtained from T2DM patients (8-OH-dG, red; c-kit, green; cTnI, white; DAPI, blue; n=10 T2DM heart sections and n=6 NDM heart sections). Scale bars=50μm and 10μm respectively (**B**) Representative light microscopy, bar graph and confocal image showing 3-NT positive cardiomyocytes (3-NT, brown) and 3-NT positive hCSCs in LV samples obtained from T2DM and NDM patients (3-NT, red; c-kit, green; DAPI, blue; n=10 T2DM heart sections and n=6 NDM heart sections). Scale bar=100μm and 10μm respectively. (**C**) Bar graph and representative confocal images showing $p16^{INK4a}$ expression in c-$kit^{pos}CD45^{neg}CD31^{neg}$ hCSC-enriched cardiac cells in LV samples obtained from T2DM patients compared to NDM counterparts ($p16^{INK4a}$, red; c-kit, green; DAPI, blue; n=10 T2DM heart sections and n=6 NDM heart sections). Scale bar=10μm. All data are mean±S.D.

Figure 3. Phenotypic characterization of c-$kit^{pos}CD45^{neg}CD31^{neg}$ T2DM-hCSCs *in vitro*. (**A**) Flow cytometry dot plots showing reactive oxygen species in T2DM-hCSCs compared to NDM-hCSCs (Representative of n=3 experiments). (**B**) Bar graphs showing a telomerase activity and average telomere length in c-$kit^{pos}CD45^{neg}CD31^{neg}$ T2DM-hCSCs compared to NDM-hCSCs. (n=6 number of biological replicates). All data are mean±S.D. (**C**) Representative Western Blot showing $p16^{INK4a}$, p21 and p53 levels in T2DM-hCSCs compared to NDM-hCSCs (Representative of n=3 biological replicates). (**D**) Bar graph and representative confocal microscopy images from cytospin preparations showing $p16^{INK4a}$ expression (red) in c-$kit^{pos}CD45^{neg}CD31^{neg}$ T2DM-hCSCs compared to NDM-hCSCs. Scale bar=75μm (n=6 biological replicates). (**E**) Representative confocal microscopy images from cytospin preparation of c-$kit^{pos}CD45^{neg}CD31^{neg}$ T2DM-hCSCs co-expressing the senescent markers $p16^{INK4a}$ (green) and p21 (red). Scale bar=75μm. (n=6 number of biological replicates). (**F**) Bar graph and representative light microscopy images showing senescence-associated β-Gal positive cells (blue) in T2DM-hCSCs compared to NDM-hCSCs. Scale bar=200μm. (n=6 biological replicates). (**G,H**) Bar graphs and representative confocal microscopy images from cytospin preparations of c-$kit^{pos}CD45^{neg}CD31^{neg}$ T2DM-hCSCs and NDM-hCSCs showing (**G**) the expression of γ-H2AX, (green) and (**H**) TdT (green) in T2DM-hCSCs compared to NDM-hCSCs. Scale bars=75μm and 50μm (n=6 biological replicates). All data are mean±S.D.

Figure 4. Impaired cell growth and myogenic differentiation potential of T2DM-hCSCs *in vitro.* (**A**) Cell growth curve shows a decreased proliferation *in vitro* of c-$kit^{pos}CD45^{neg}CD31^{neg}$ T2DM-hCSCs compared to NDM-hCSCs (n=6 biological replicates). (**B-D**) Bar graphs showing respectively BrdU incorporation, clonogenesis and spherogenesis in c-$kit^{pos}CD45^{neg}CD31^{neg}$ T2DM-hCSCs compared to NDM-hCSCs (n=6 biological replicates). (**E**) Heat maps showing qRT- PCR analysis of the main cardiac transcription factors and myocyte contractile genes in c-$kit^{pos}CD45^{neg}CD31^{neg}$ T2DM-hCSCs compared with NDM-hCSCs after myogenic differentiation induction. Color scale indicates change in Ct (threshold cycle) relative to the normalized GAPDH control (Representative of n=3 biological replicates). (**F**) Bar graph and confocal images showing actinin (red) expression levels of differentiated T2DM-hCSCs compared to NDM-hCSCs. Scale bar=200μm (n=6 biological replicates). (**G**) Bar graph and confocal images showing cTnI (red) expression levels of differentiated T2DM-hCSCs compared to NDM-hCSCs. Scale bar=200μm (n=6 biological replicates). All data are mean±S.D.

Figure 5. The senescence-associated secretory phenotype (SASP) of T2DM-hCSCs. (A) Bar graphs showing the SASP factor protein levels in culture media from T2DM-hCSCs and NDM-hCSCs after 24 hours in serum-free conditions (n=3 biological replicates). (**B**) Bar graphs showing transcript SASP factor expression in T2DM-hCSCs vs. NDM-hCSCs (n=3 biological replicates). (**C**) Cell growth curve showing the *in vitro* proliferative change of NDM-hCSCs placed in conditioned medium (CoMe) derived from T2DM-hCSCs compared to the NDM-hCSCs placed in unconditioned medium (UnCoMe) and NDM-hCSCs CM (n=6 number of biological replicates). (**D**) Bar graph showing BrdU incorporation of NDM-hCSCs placed in UnCoMe, NDM-CoMe and T2DM-CoMe (n=6 biological replicates). (**E**) Bar graphs showing senescent $p16^{INK4a}$ positive hCSCs, SA-β-gal-positive hCSCs and γ-H2AX-positive hCSCs in NDM-hCSCs treated with T2DM-CoMe compared to UnCoMe and NDM-CoMe (n=6 biological replicates). (**F**) Bar graphs showing the number of $p16^{INK4a}$ and β-Gal positive NDM-hCSCs under HG condition *in vitro* compared to NDM-hCSCs grown in LG condition (n=6 biological replicates). (**G**) Bar graphs showing transcript SASP factors expression NDM-hCSCs under HG condition *in vitro* compared to NDM-hCSCs grown in LG condition (n=3 biological replicates). (**H**) Bar graphs showing expansion capacity of NDM-hCSCs under HG condition *in vitro* compared to NDM-hCSCs grown in LG condition (n=6 biological replicates). All data are mean±S.D

Figure 6. Senolytics ameliorates regenerative deficit of diabetic hCSCs. (A) Light microscopy images showing that the typical enlarged and flattened morphology of senescent cells present in untreated control (CTRL) disappear in D+Q treated T2DM-hCSCs *in vitro*. Scale bar=400μm **(B)** Cell growth curve shows the *in vitro* proliferation of c-$kit^{pos}CD45^{neg}CD31^{neg}$ T2DM-hCSCs after D+Q treatment compared to CTRL *per se* (n=6 biological replicates). **(C-E)** Bar graphs showing the number of **(C)** β-Gal, **(D)** $p16^{INK4a}$ senescent cells and **(E)** γ-H2AX positive cells in T2DM-hCSCs after D+Q treatment compared to CTRL (n=6 biological replicates). **(F)** Bar graphs showing transcript SASP factor expression in T2DM-hCSCs after D+Q treatment vs. CTRL (n=3 biological replicates). **(G)** Heat maps showing qRT-PCR analysis of the main cardiac transcription factors and myocyte contractile genes (GATA-4, NKX2.5, MEF2C, TNNT2, ACTC1, MYH6 and MYH7) in differentiating T2DM-hCSCs after D+Q treatment vs. CTRL. Color scale indicates change in Ct (threshold cycle) relative to the normalized GAPDH control (Representative of n=3 biological replicates). (**H**) Bar graphs show the percentage of cTnI expressing cells in differentiated T2DM-hCSCs after D+Q treatment vs. CTRL (n=6 biological replicates). All data are mean±S.D

Figure 7. Diabetic status causes myocardial cell senescence with myocardial pathologic remodeling and cardiac dysfunction. (A) Representative pulsed wave Doppler Mitral Velocity tracing (PW MV) and representative pulsed wave tissue Doppler imaging velocity tracing (PW TDI) of T2DM vs CTRL (normal chow diet, NCD and high fat diet, HFD) mice. (NCD, n=9; HFD, n=9; T2DM, n=18). (**B**) Violin plots represent cumulative E/A ratio (left) and E/E' ratio (right) in T2DM vs CTRL (NCD and HFD) mice. (NCD, n=9; HFD, n=9; T2DM, n=18). (**C**) Bar graph and confocal images of Dihydroethidium (DHE) detection in heart frozen section from CTRL and T2DM mice. Scale bar=25μm (n=6 biological replicates). (**D**) Bar graph and representative confocal images showing $p16^{INK4a}$ positive nuclei in myocardial (interstitial) cell in T2DM mice compared to CTRL mice. Scale bar=8μm (left panel) and 5μm (right panel) (n=6 biological replicates). (**E**) Bar graph and representative confocal images of apoptotic TdT (green) positive cardiomyocytes nuclei in T2DM mice compared to CTRL mice. Scale bar=8μm. (n=6 biological replicates). (**F**) Representative light microscopy of Picro Sirius Red Staining of T2DM mice compared to CTRL mice. Scale bar=200μm. (n=6 biological replicates). (**G**) Bar graph and representative confocal images of cardiac cross-section showing cardiomyocyte hypertrophy in T2DM mice when compared with CTRL mice (WGA, wheat germ agglutinin, Cy5 staining, and white fluorescence; cTnI, green; DAPI, blue nuclei). Scale bar=25 μm. (n=6 biological replicates). (**H**) Bar graph and confocal images showing the percentage of $p16^{INK4a}$ positive CSCs in T2DM mice compared to CTRL mice. (n=6 biological replicates). All data are mean±S.D

Figure 8. Senolytics treatment *in vivo* removes senescent CSCs and improves cardiac repair and regeneration in diabetic mice. (A) Representative pulsed wave Doppler Mitral Velocity tracing (PW MV) and representative pulsed wave tissue Doppler imaging velocity tracing (PW TDI) in D+Q treated T2DM mice compared to vehicle treated mice. (CTRL*, n=9; Vehicle, n=9; D+Q, n=9). (**B**) Violin plots represent cumulative E/A ratio (left) and E/E' ratio (right) in D+Q treated diabetic mice compared to vehicle treated mice. (CTRL*, n=9; Vehicle, n=9; D+Q, n=9). (**C**) Bar graphs showing transcript SASP factor expression in CSCs isolated from vehicle and D+Q treated T2DM mice compared to CSCs isolated from CTRL mice. (n=3 biological replicates). (**D**) Heat maps showing the myogenic differentiation of CSCs isolated from vehicle or D+Q-treated T2DM mice compared to CSCs from CTRL mice. (n=3 biological replicates). (**E**) Bar graph and representative confocal microscopy images of BrdU positive cardiomyocytes (arrowhead indicates BrdU positive cardiomyocytes, green; cTnI, red; PCM1, white; DAPI, blue nuclei) in D+Q-treated T2DM mice compared vehicle-treated mice heart sections. Scale bar=25 μm. (n=6 biological replicates). All data are mean±S.D

* *Considering that CTRL mice fed with NCD or HFD had undistinguishable cardiac systolic and diastolic function and their cardiac histology and CSC content, phenotype and function was comparable (data not shown), only the HFD mice are presented in this figure as CTRL*

Figure 1

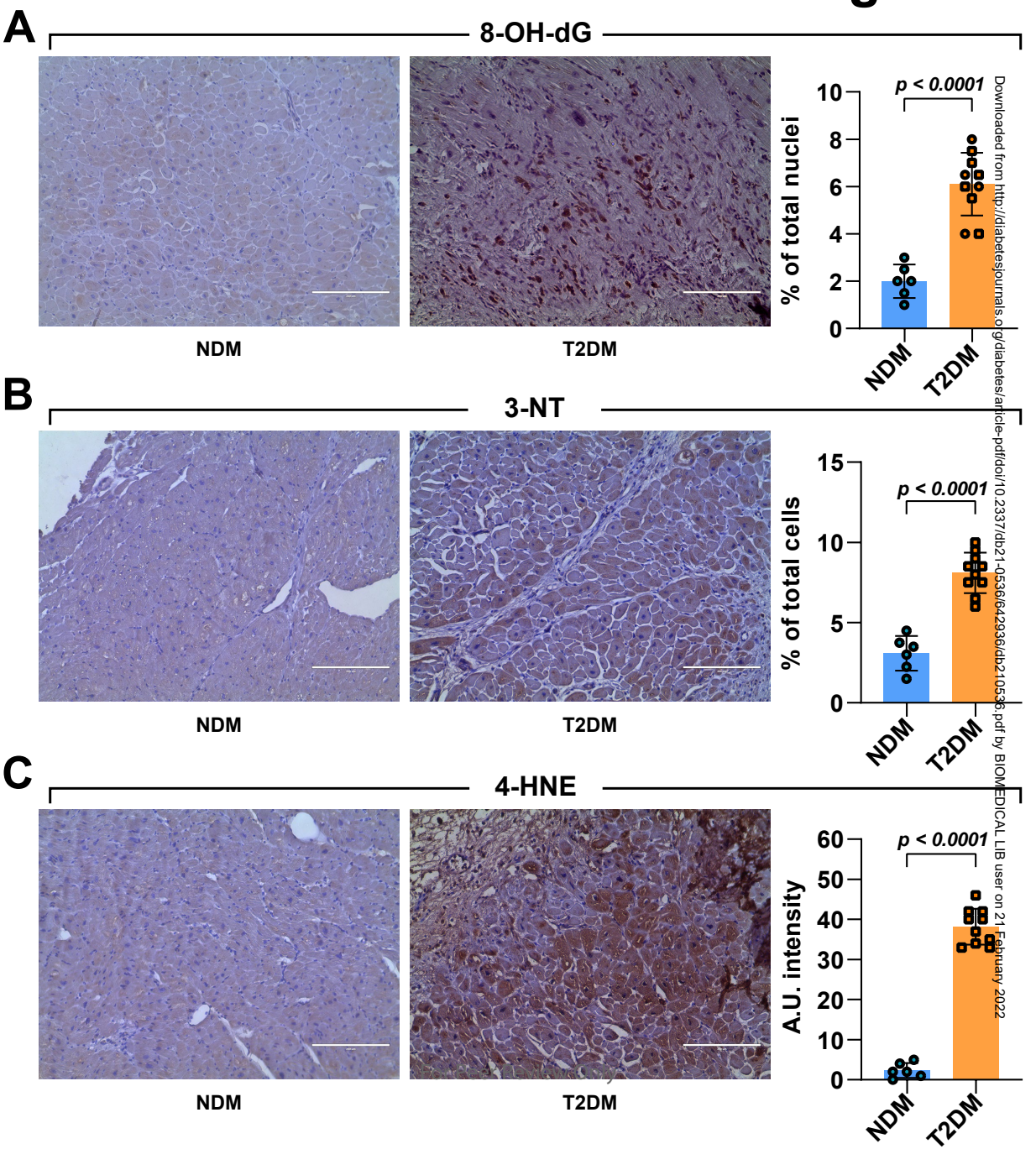

Figure 2

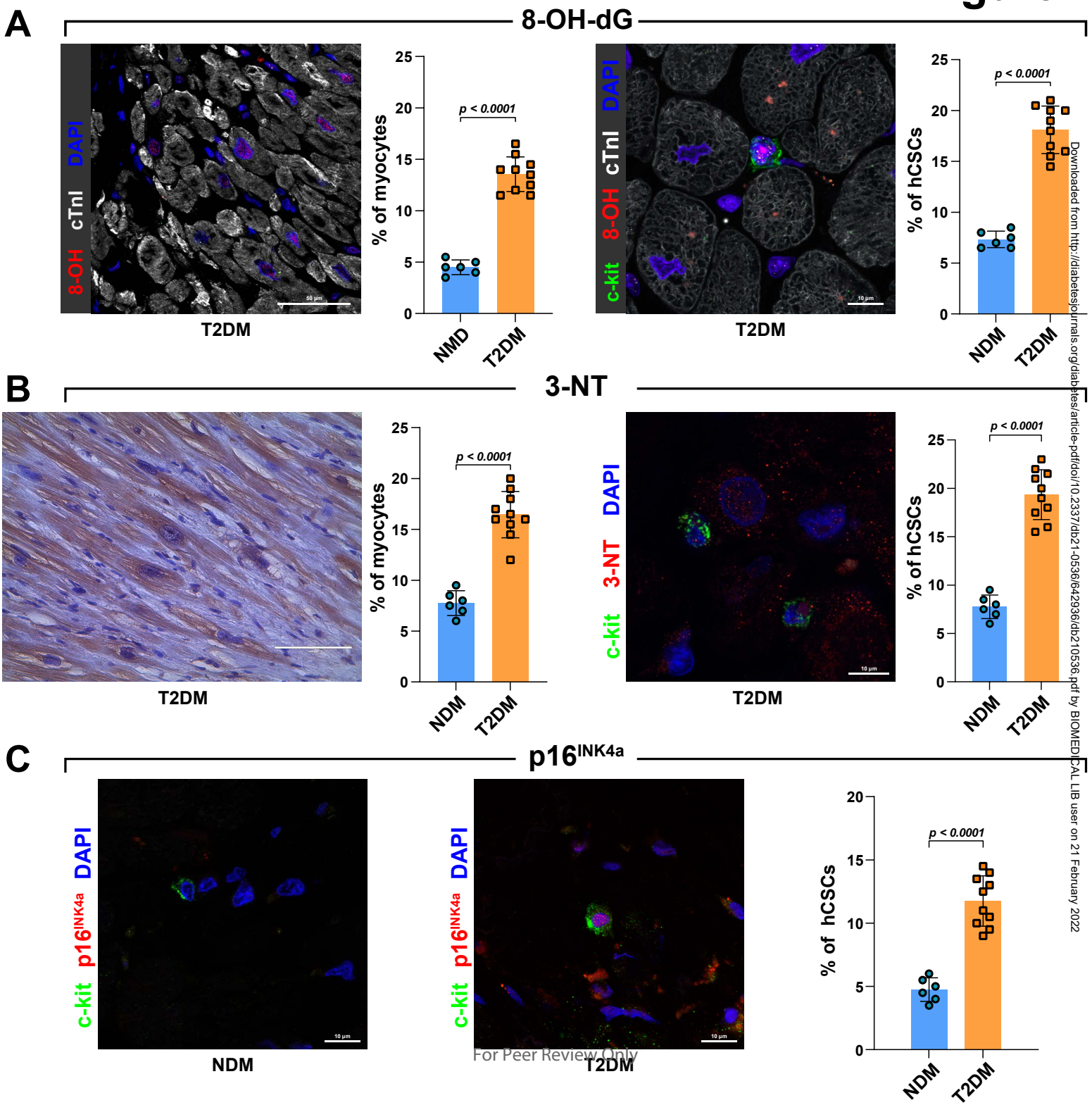

Figure 3

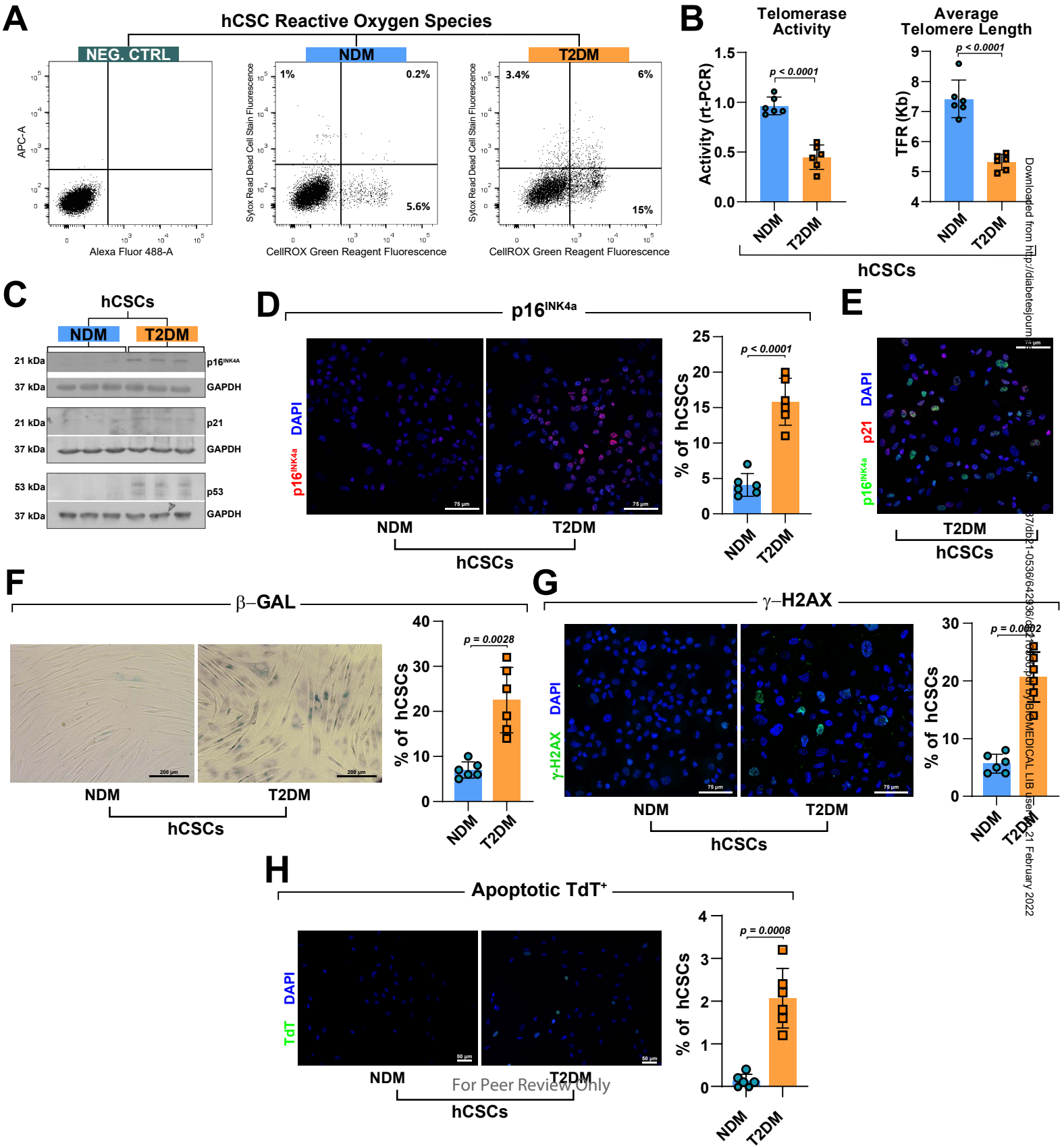

Figure 4

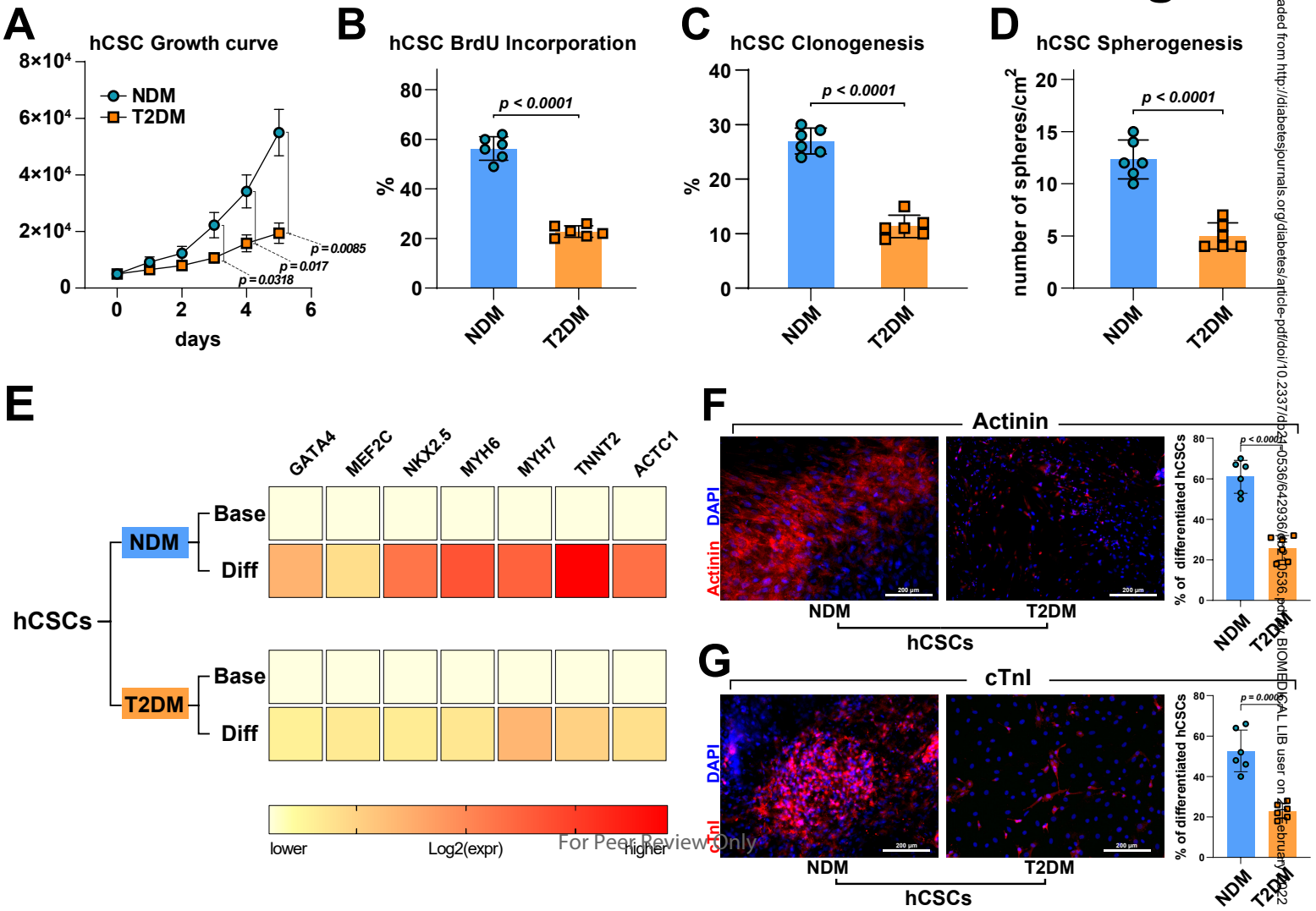

Figure 5

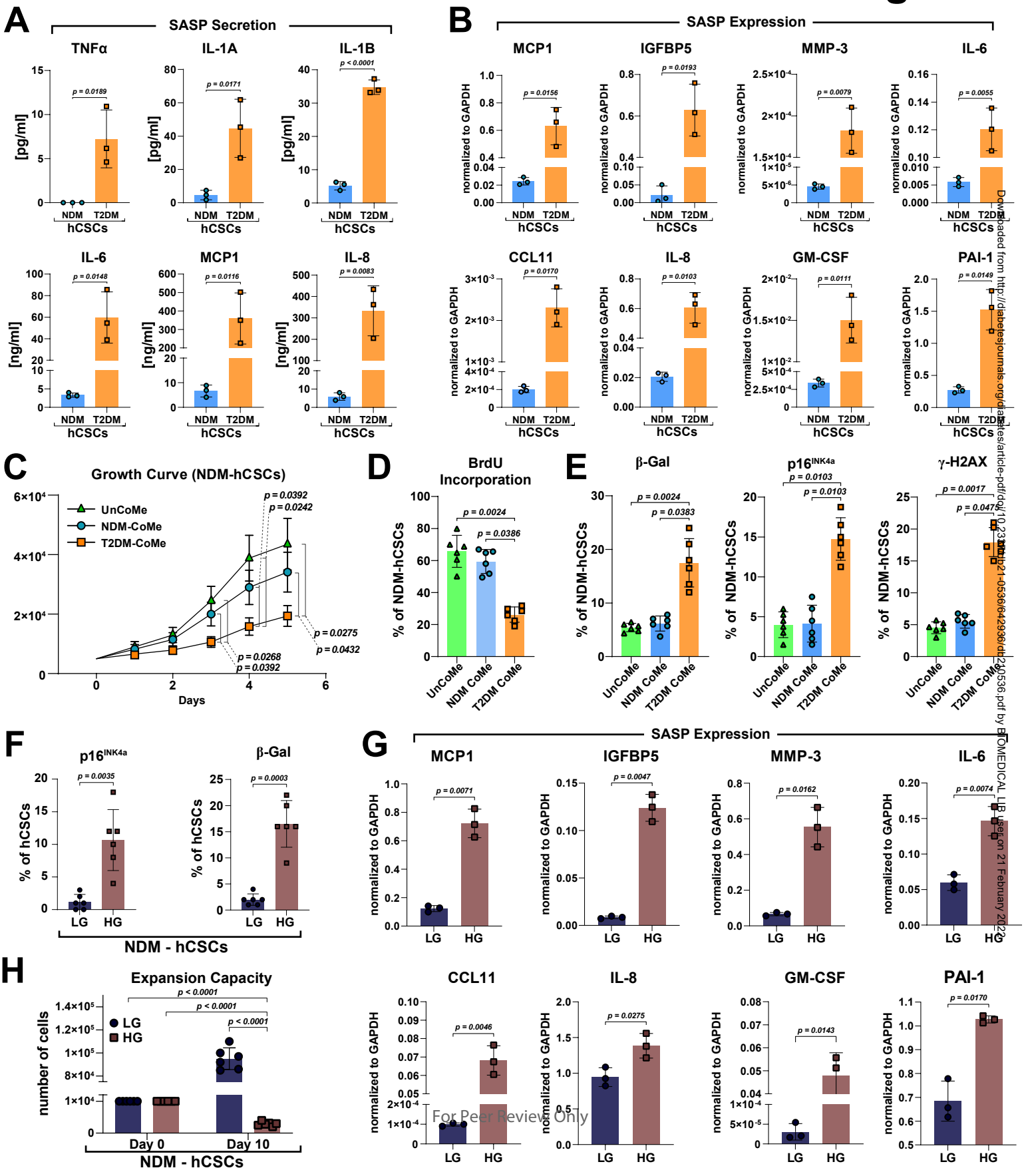

Figure 6

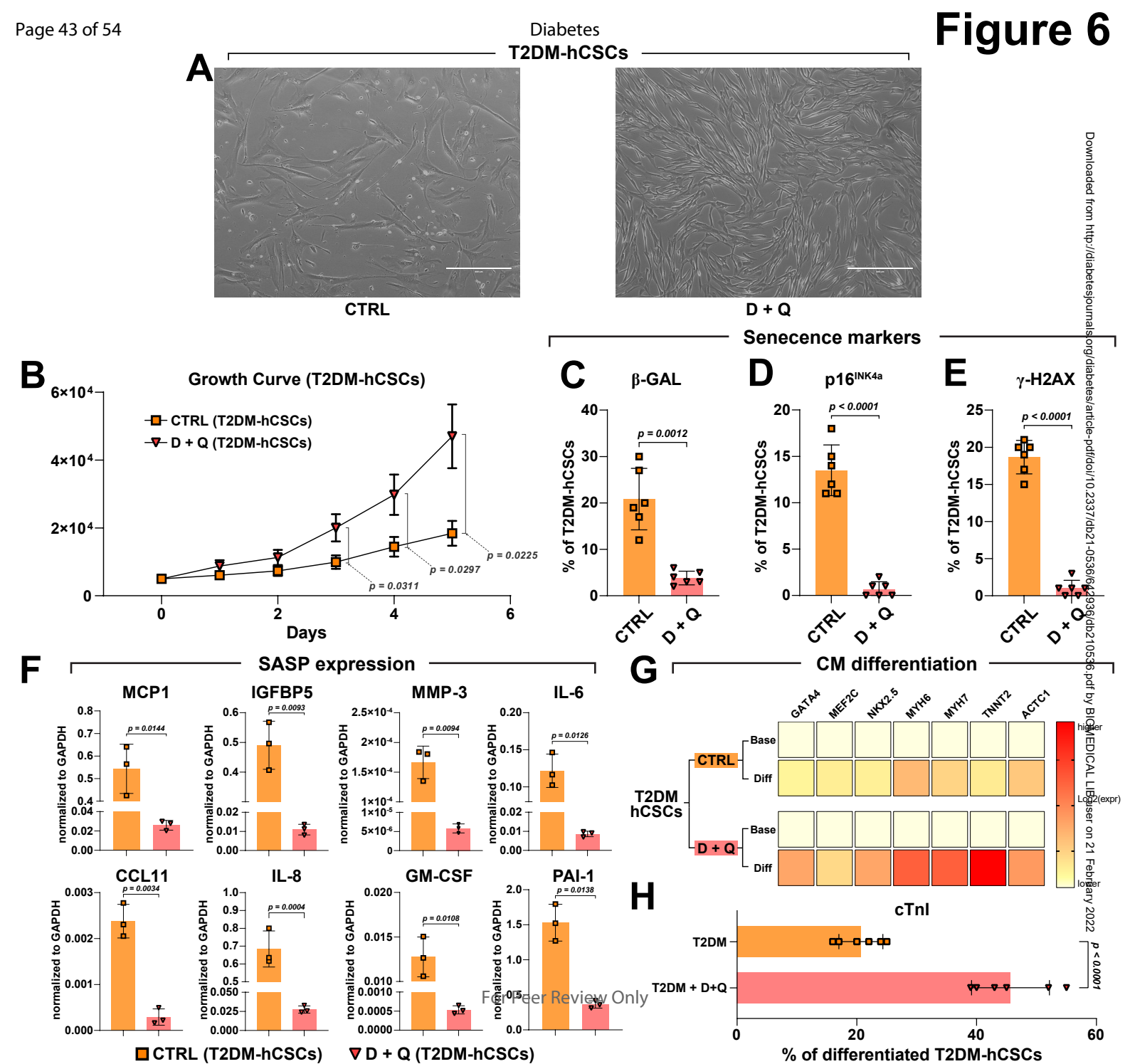

Figure 7

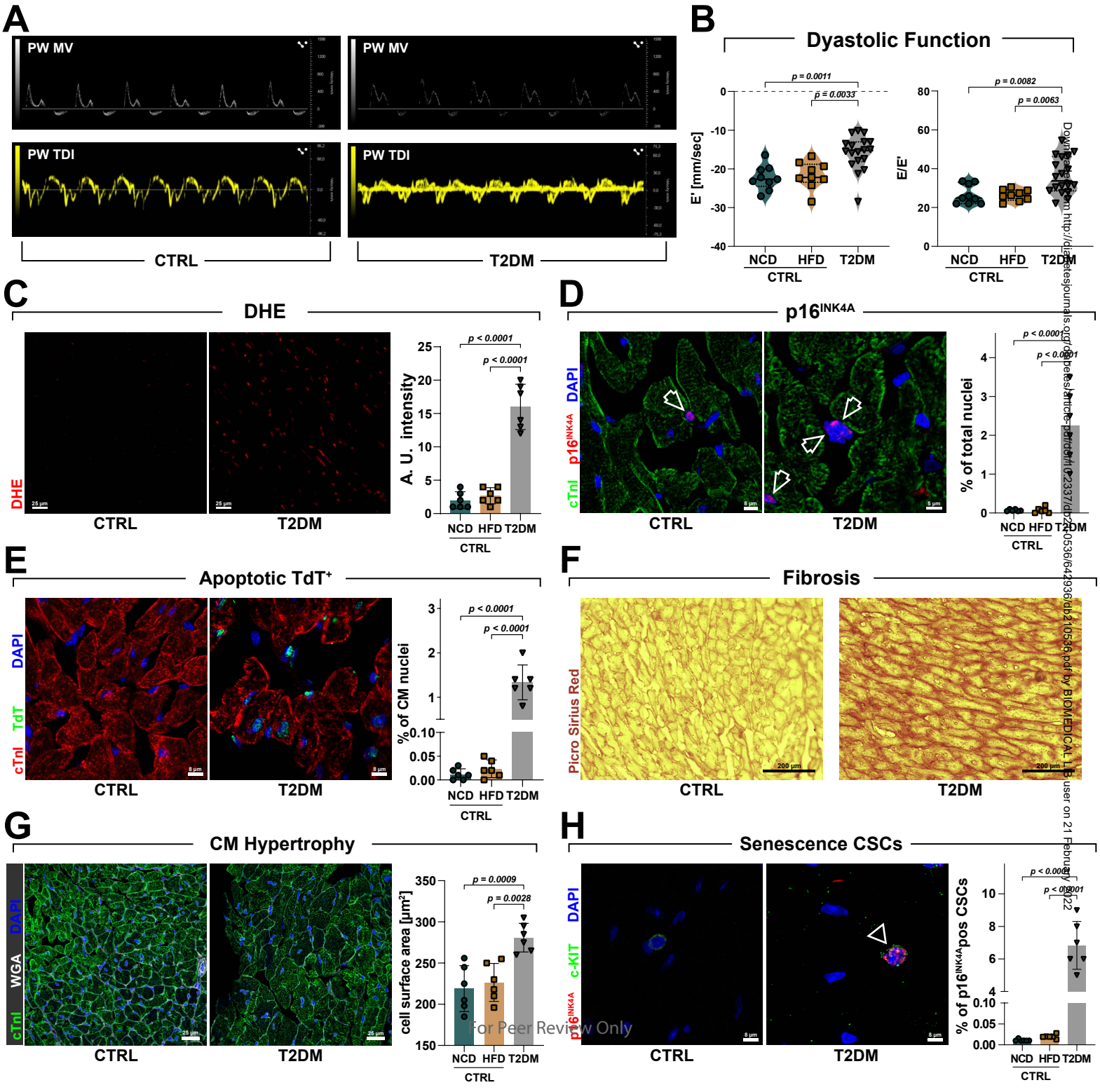

Figure 8

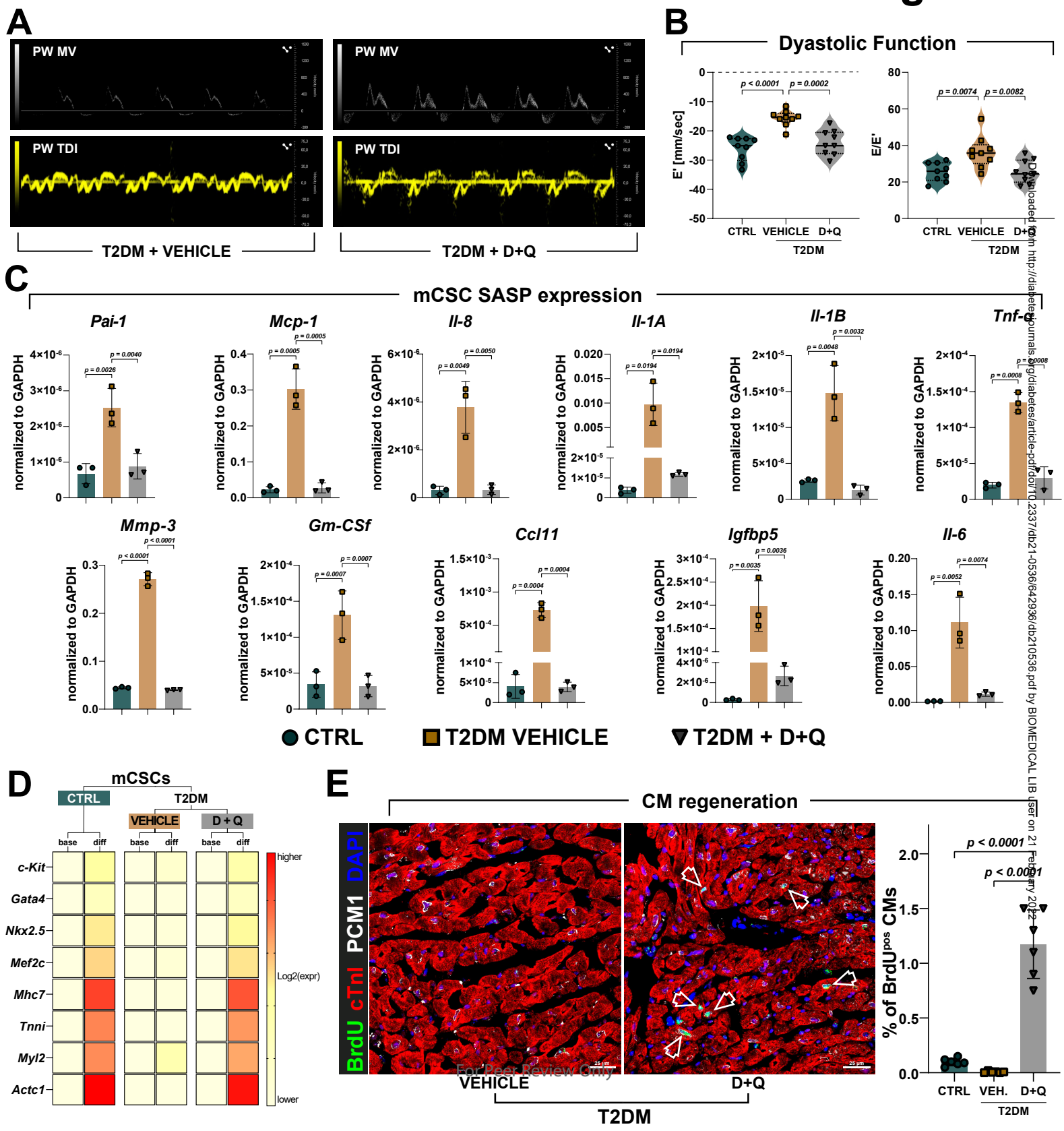

Online supplemental/appendix file

Diabetes-induced Cellular Senescence and Senescence-Associated Secretory Phenotype Impair Cardiac Regeneration and Function Independently of Age

Fabiola Marino1,2,#, Mariangela Scalise1#, Nadia Salerno3, Luca Salerno1, Claudia Molinaro3, Donato Cappetta4, Michele Torella5, Marta Greco1, Daniela Foti1, Ferdinando C. Sasso5, Pasquale Mastroroberto1, Antonella De Angelis4, Georgina M. Ellison-Hughes6, Maurilio Sampaolesi2, Marcello Rota7, Francesco Rossi4, Konrad Urbanek1, Bernardo Nadal-Ginard3, Daniele Torella1*, Eleonora Cianflone3,7*

Supplementary Figure 1

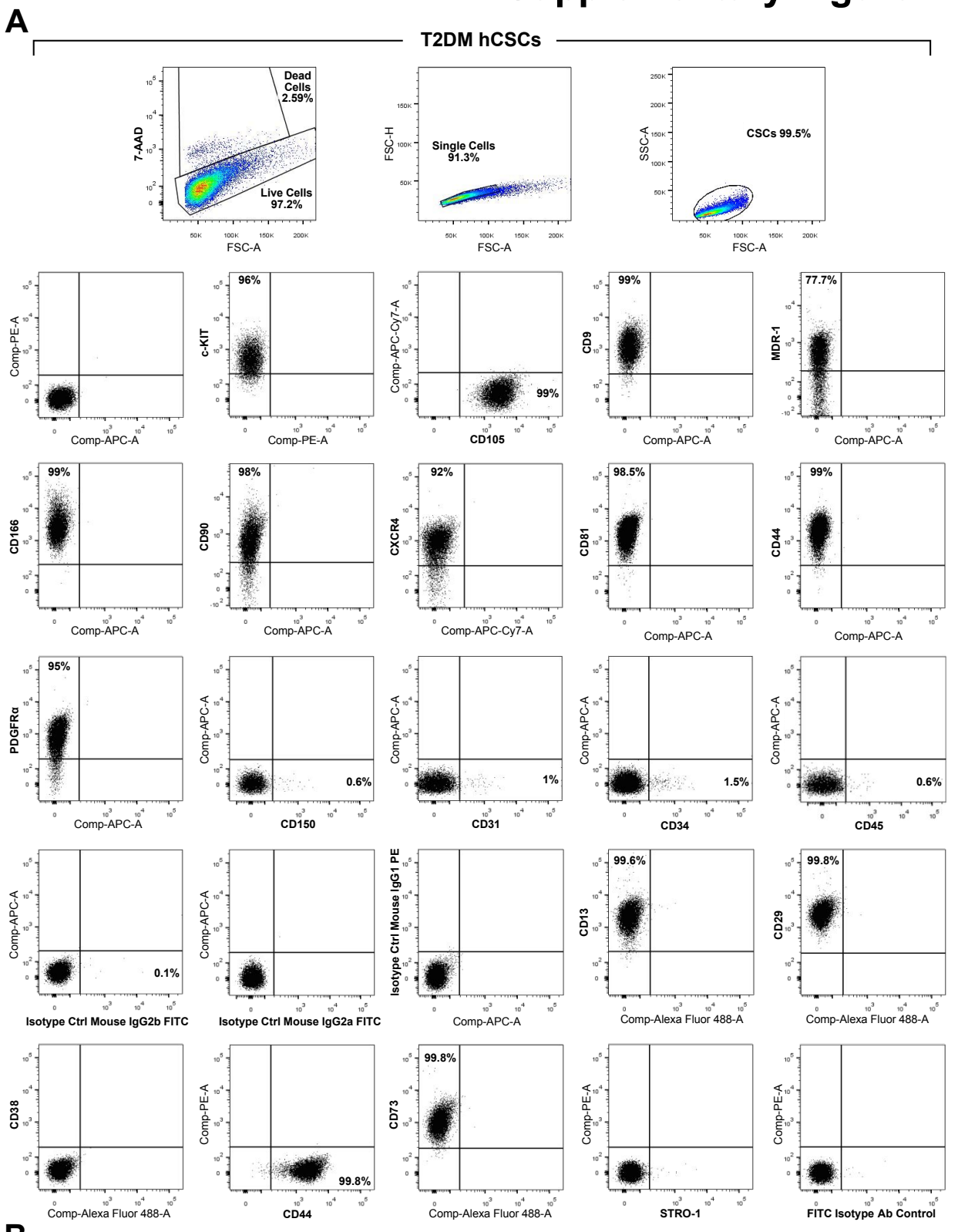

Supplementary Figure 1. (**A**) Flow cytometry dot plots showing the gating strategy used to evaluate the membrane phenotype of c-kit^{pos}CD45^{neg}CD31^{neg} T2DM-hCSCs and their differential surface marker expression (Representative of n=3 biological replicates). (**B**) Representative confocal microscopy images from cytospin preparation of c-kit^{pos}CD45^{neg}CD31^{neg} T2DM-hCSCs expressing the pluripotency markers OCT4, SOX2, NANOG, KLF4, cMYC and Sac. Scale bar=75μm. (OCT4, SOX2, NANOG, KLF4, cMYC, Sac2, green; DAPI, blue; Representative of n=3 number of biological replicates). All data are mean±S.D

Supplementary Figure 2

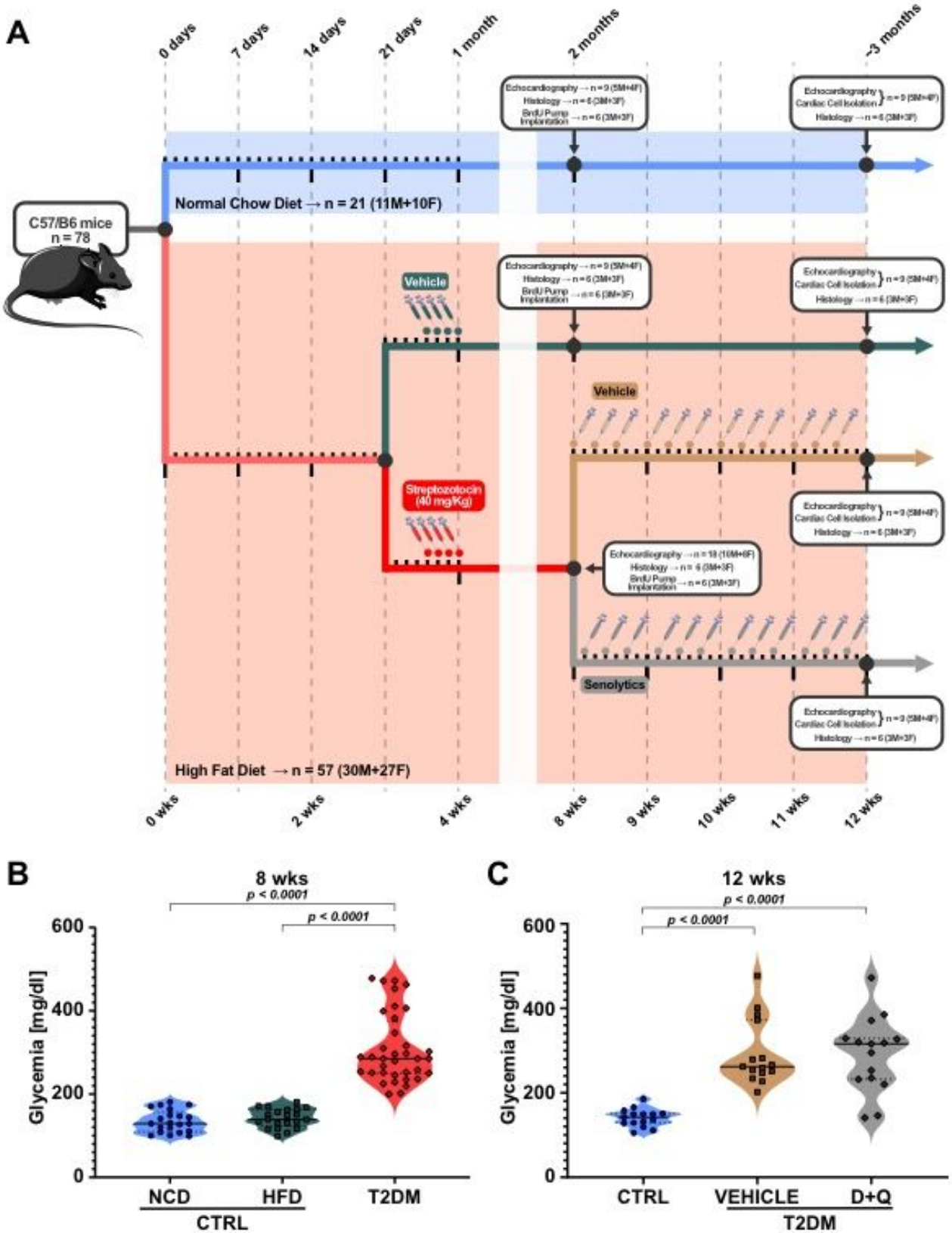

Supplementary Figure 2. (**A**) Schematic representation of the *in vivo* study. (**B**) Violin plots showing the measurements of glycemia respectively at 8 weeks in CTRL (NCD and HFD) and T2DM mice and T2DM (NCD, n=21 ; HFD, n=21; T2DM, n=36), and at 12 weeks in CTRL, Vehicle and D+Q treated mice (CTRL, n=15; Vehicle, n=15; D+Q, n=15).

Supplementary Figure 3

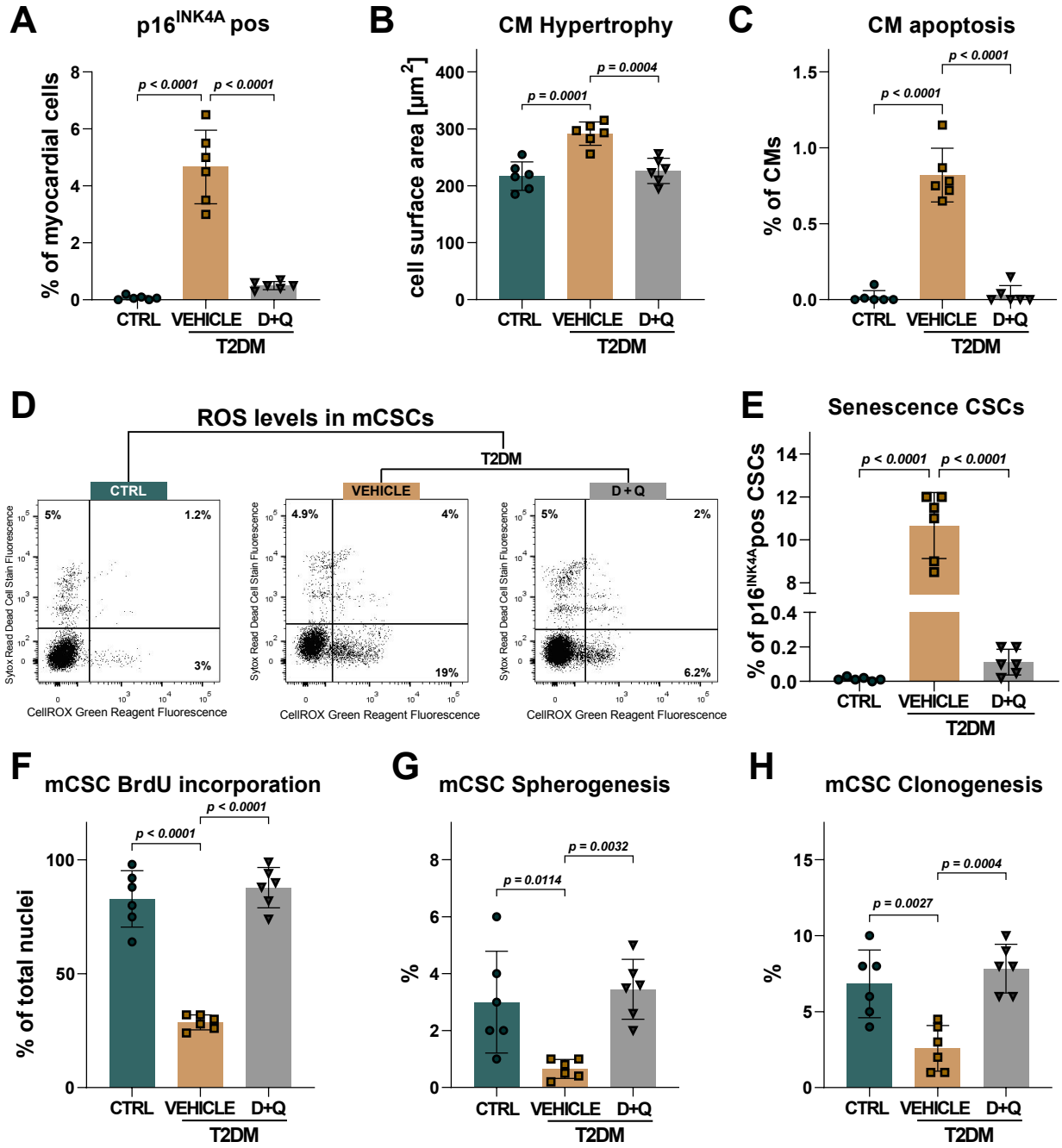

Supplementary Figure 3. (A-C) Bar graphs showing the percentage of myocardial cells p16^{INK4a} positive (**A**), CM size and hypertrophy (**B**), apoptotic TdT positive cardiomyocytes (**C**) in T2DM mice treated with D+Q senolytic combination compared to vehicle treated mice and CTRL mice. (n=6 biological replicates). (**D**) The ROS levels were assessed by determining CellROX fluorescence intensity by flow cytometry on CSCs obtained from CTRL, vehicle or D+Q-treated T2DM mice (Representative of n=3 biological replicates). (**E**) Bar graphs showing the percentage of CSCs p16^{INK4a} positive in T2DM mice treated with D+Q senolytic combination compared to vehicle treated mice and CTRL mice. (n=6 biological replicates). (**F-H**) Bar graphs showing the *in vitro* proliferation potential (**F**) spherogensis (**G**) and clonogenesis (**H**) of CSCs isolated from vehicle or D+Q-treated T2DM mice compared to CSCs from CTRL mice (n=6 biological replicates). All data are mean±S.D

Supplementary Table 1. Characteristics of the Patients Enrolled in the Study

	T2DM Patients n=16	NDM Patients n=12	
Sex, M/F	14/2	11/1	0.54
Age, y	59.4±4.0	59.4±4.1	0.97
Duration of diabetes, y	7.3±4.3	-	
BMI, kg/m^2	27.7±3.1	28.8±3.5	0.39
HbA_{1c}, %	9.1±3.8	-	
FBG, mg/dl	166.4±64.1	92.7±9.3	<0.01
LDL cholesterol, mg/dl	108.6±48.3	118.4±43.1	0.58
HDL cholesterol, mg/dl	41±15.4	47.2±17.0	0.33
TG, mg/dl	168.9±106.5	139.7±67.4	0.38
SBP, mm Hg	133.6±14.7	131.2±19.0	0.75
DBP, mm Hg	79.2±9.1	79.7±11.0	0.91
Three-vessel CHD, n	8	8	0.67
Two-vessel CHD, n	5	4	0.92
Therapy, n			
Statins	16	12	
Aspirin	16	12	
ß-Blockers	16	10	0.31
ACEIs/ARBs	16	10	0.29
Nitrates	0	0	

Quantitative data are expressed as mean±SD. Binary data are reported by counts. *P<0.01 vs DM patients. Comparisons of the quantitative data have been made through use of Student's t test for independent samples. The $\chi 2$ test was used to compare binary data. T2DM indicates Type 2 Diabetes Mellitus; NDM non diabetes Mellitus; BMI body mass index; FBG, fasting blood glucose; LDL, low-density lipoprotein; HDL, high-density lipoprotein; TG, triglycerides; SDP, systolic blood pressure; DBP, diastolic blood pressure; CHD, coronary heart disease; ACEI, angiotensin-converting enzyme-inhibitor; ARB, angiotensin II receptor blocker.

Supplementary Table 2: Antibodies

Antigen	Antibody ID	Company	Application
c-kit		Dako	IF
c-kit		SantaCruz Biotech	IF
p16		SantaCruz Biotech	IF, WB
p53		SantaCruz Biotech	WB
p21		SantaCruz Biotech	WB
p21		Abcam	IF, IHC
8-OH		Origene	IF
3-NT		Thermo Fisher	IF, IHC
4-HNE		Abcam	IF, IHC
cTNI		Abcam	IF
g-H2AX		Cell Signaling	IF
cTNI		Abcam	IF
Actinin		Abcam	IF
WGA		Thermo Fisher	IF
BrdU		Roche	IF
PCM1		AtlasAntibodies	IF
TdT		Invitrogen	IF
Oct-4		SantaCruz Biotech	IF
Nanog		R&D Sistems	IF
Klf-4		Invitrogen	IF
Sox-2		SantaCruz Biotech	IF
Sac-2		SantaCruz Biotech	IF
Gapdh		Bioss	WB
c-kit	A3C6E2	Miltenyi Biotec	FC
CD184 (CXCR4)	12G5	Miltenyi Biotec	FC
CD9	SN4 C3-3A2	Miltenyi Biotec	FC
CD44	DB105	Miltenyi Biotec	FC
CD81	5A6	BioLegend	FC
CD90	DG3	Miltenyi Biotec	FC
CD166	3A6	BioLegend	FC
CD105	43A4E1	Miltenyi Biotec	FC
MDR-1	UIC2	BioLegend	FC
PDGFR-α	16A1	BioLegend	FC
CD150	REA151	Miltenyi Biotec	FC
CD31	AC128	Miltenyi Biotec	FC
CD45	REA747	Miltenyi Biotec	FC
CD73	AD2	Miltenyi Biotec	FC
CD38	HIT2	BD Pharmigen	FC
CD29	TS2/16	Miltenyi Biotec	FC
CD44	DB105	Miltenyi Biotec	FC
CD13	REA263	Miltenyi Biotec	FC
STRO-1		Santa Cruz Biotech	FC
CD34	AC136	Miltenyi Biotec	FC

Mouse IgG1 - Isotype control antibody		Miltenyi Biotec	FC
Mouse IgG2a - Isotype control antibody		Miltenyi Biotec	FC
Mouse IgG2b - Isotype control antibody		Miltenyi Biotec	FC
AlexaFluor488 anti-mouse IgG		Invitrogen	FC

FC denotes Flow Cytometry, IF denotes Immunofluorescence, WB denotes Western Blot and IHC denotes Immunoistochemistry

Table 3. RT-PCR Primers

Taqman Primers List

GENE	SPECIES	ID NUMBER
hGAPDH	Human	Hs02758991_g1
hMEF2C	Human	Hs00231149_m1
hGata4	Human	Hs00171403_m1
hNkx2.5	Human	Hs00231763_m1
hMyh6	Human	Hs01101425_m1
hMyh7	Human	Hs01110632_m1
hTnnt2	Human	Hs00165960_m1
hACTC1	Human	Hs01109515_m1
hCCL2	Human	Hs00234140_m1
hIL-8	Human	Hs00174103_m1
hGM-CSF	Human	Hs00929873_m1
hIGFBP5	Human	Hs00181213_m1
hIL-6	Human	Hs00174131_m1
hPAI-1	Human	Hs00167155_m1
hMMP-3	Human	Hs00968305_m1
hCCL11	Human	Hs00237013_m1
Gapdh	Mouse	Mm99999915_g1
Mef2c	Mouse	Mm01340842_m1
Nkx2.5	Mouse	Mm01309813_s1
Gata4	Mouse	Mm00484689_m1
c-kit	Mouse	Mm00445212_m1
Myh7	Mouse	Mm01319006_g1
Myl2	Mouse	Mm00440384_m1
TnnT2	Mouse	Mm01290256_m1
Actc1	Mouse	Mm01333821_m1

List of mouse gene-specific primer sets for SYBR Green qPCR

GENE	**Forward Primer**	**Reverse Primer**
MCP1 (CCL2)	5'-GCTACAAGAGGATCACCAGCAG-3'	5'-GTCTGGACCCATTCCTTCTTGG-3'
IGFBP5	5′-AACGAAAAGAGCTACCGCGA-3′	5′-CCGACAAACTTGGACTGGGT-3′
PAI-1	5′-GGCCATTACTACGACATCCTG-3′	5′-GGTCATGTTGCCTTTCCAGT-3′
GM-CSF	5'-AACCTCCTGGATGACATGCCTG-3'	5'-AAATTGCCCCGTAGACCCTGCT-3'
IL-8	5′-GTGCAGTTTTGCCAAGGAGT-3′	5′-TTATGAATTCTCAGCCCTCTTCAAAAACTT CTC-3′
CCL11	5'-TGCAGAGCTCCACAGCGCTT-3'	5'-GGGTGAGCCAGCACCTGGGA-3'
IL-6	5′-TGAGAAAAGAGTTGTGCAATGG-3′	5′-GGTACTCCAGAAGACCAGAGG-3′
MMP-3	5′-GTTGGAGAACATGGAGACTTTGT-3′	5′-CAAGTTCATGAGCAGCAACCA-3′
IL1a	5′-AGGGAGTCAACTCATTGGCG-3′	5′-TGGCAGAACTGTAGTCTTCGT-3′
IL1b	5′-TGCCACCTTTTGACAGTGATG-3′	5′-TGATGTGCTGCTGCGAGATT-3′
TNFα	5'-GCAGGTTCTGTCCCTTTCAC-3'	5'-GTCGCGGA TCA TGCTTTCTG-3'

Supplementary Table 4. Echocardiography data for figures 7-8.

	Sex	BW (gr)	LVEDD (mm)	LVESD (mm)	EF (%)	FS (%)	HR (bpm)	E velocity mm/s	A velocity	E/A	E' velocity	E/E'
8 weeks												
NCD	5M+4F	21±0.5	3,84±0.17	2,70±0.13	57,26±3.57	29,63±2.37	449±49	585,56±67,20	307,22±62.4	1,94±0.29	22,28±2.57	26,70±1.75
HFD	5M+4F	25±2*	3,79±0.32	2,53±0.36	62,56±7.21	33,52±5.46	416±28	566,08±79.63	298,63±90.43	2,00±0.46	21,63±3.5	26,39±2.9
T2DM	10M+ 8F	22±1	3,895±0.34	2,77±0.39	56,28±7.28	29,145±4.84	425±55	550,048±103.56	349,79±116.22	1,72±0.58	15,89±4.45*	36,29±9.41#
12 weeks												
CTRL (HFD)	5M+4F	28±1.5	3,74±0.23	2,49±0.29	62,80±6.20	33,50±4.42	421±42	661,92±180.19	379,55±96.53	1,770±0.31	26,17±4.40	25,42±5.44
T2DM+ Vehicle	5M+ 4F	23±1.5*	3,99±0.21	2,81±0.25	57,03±4.9	29,59±3,29	427±52	554,80±89.25	359,35±110.34	1,66±0.52	15,68±2.72*	36,34±8.75#
T2DM+ (D+Q)	5M+ 4F	24±0.5	3,63±0.30	2,38±0.18	64,098±3.42	34,26±2.65	450±47	606,11±136.93	365,24±106,30	1,72±0.37	24,08±4.23	25,61±6.33

BW= body weight

LVEDD= left ventricular-end-diastolic diameter

LVESD= left ventricular-end-systolic diameter

EF= ejection fraction

FS= fractional shortening

HR= heart rate

8 weeks p-values: BW*= p<0.01 vs NCD and T2DM; E' velocity*= p<0.003 vs HFD and NCD; E/E'#= p<0.008 vs HFD and NCD.

8 weeks p-values: BW*= p<0.01 vs NCD and T2DM; E' velocity*= p<0.0002 vs CTRL and T2DM+(D+Q); E/E'#= p<0.008 vs CTRL and T2DM+(D+Q).